Research Report PIBMRI 1151-63
Contract No. AFOSR-62-295

THE ELECTROMAGNETIC FIELDS OF CERTAIN UNIAXIALLY ANISOTROPIC DIELECTRIC SLABS

by

Frank M. Labianca

Polytechnic Institute of Brooklyn
Microwave Research Institute
55 Johnson Street
Brooklyn 1, New York

Report PIBMRI-1151-63
Contract No. AFOSR-62-295

9 April 1963

Title Page
Acknowledgment
Abstract
Table of Contents
Table of Figures
41 pages of text

Frank M. Labianca
Instructor

Approved: M. Schwartz
Mischa Schwartz
Head, Electrical Engineering Dept.

for
The Air Force Office of Scientific Research
The U. S. Army Research Office
The Office of Naval Research

ACKNOWLEDGMENT

The author is indebted to his late advisor, Professor Leonard O. Goldstone, for his guidance and encouragement through the final stages of the work described herein. Thanks are also due to Mr. Paul J. Crepeau, the author's present advisor, for his many helpful suggestions, and to Mr. R. Seliger, a participant in the Undergraduate National Science Foundation Education Program, for certain calculations.

The work reported herein was sponsored by the Air Force Office of Scientific Research of the Office of Aerospace Research; the department of the Army, Army Research Office; and the department of the Navy, Office of Naval Research under grant AF-AFOSR-62-295.

ABSTRACT

Two problems are considered, both of which are characterized by essentially the same geometry. In the first problem, the properties of surface waves propagating in a slab of uniaxially anisotropic dielectric are studied. The slab is of finite thickness and the relative dielectric constants of the dielectric tensor are all positive. Two cases are studied simultaneously, one being the case where the optical axis is chosen parallel to the slab, and the other being the case where the optical axis is chosen perpendicular to the slab.

Only E-mode surface waves are studied since these have the properties of extraordinary type waves. The H-mode surface waves (ordinary surface waves) have the same properties as surface waves propagating in an isotropic slab. Hence, the results for the latter problem are well known.

A transverse resonance procedure is utilized in the determination of the surface wave resonances. It is found that at any frequency the resonances are finite in number. In addition it is found that surface waves will propagate only if certain conditions are satisfied by the principal dielectric constants of the diagonal tensor.

In the second probelm the electromagnetic fields of a uniaxially anisotropic plasma slab in the presence of a magnetic line source are studied. The geometry is the same as for the first problem, except that the optical axis is chosen parallel to the slab and perpendicular to the direction of the line source. The line source is located either outside the slab or at a conducting plane (i. e., an infinite slot) covered by the slab.

Under the conditions described, it is found that the structure can support an infinite number of discrete E-mode surface waves for any frequency less than the plasma frequency. The resultant surface wave field can be expressed as a convergent series obtained by evaluating the residue terms which arise in the steepest descent representation. Furthermore it is found that all the surface waves are forward waves in so far as propagation along the slab is concerned.

In addition to the surface waves, an infinite number of nonspectral leaky wave poles is found to exist for any frequency greater than the plasma frequency. However, only a finite number of the leaky wave poles contribute residue terms for any angle of observation less than 90°, where the angle of observation is measured from the normal to the slab.

TABLE OF CONTENTS

TABLE OF FIGURES

CHAPTER I
INTRODUCTION

The problems to be considered in subsequent chapters will involve uniaxially anisotropic dielectric media. Media possessing such properties can be constructed by implanting dielectric obstacles in a suitable dielectric binder. Such obstacles would have dimensions which are small in comparison to the wavelength of the radiation and would be arranged in a geometric pattern which would give rise to the uniaxial properties. If the obstacles possess finite conductivities, the resulting artificial dielectric structure would be anisotropic both electrically and magnetically. This possibility will not be considered here. The properties of artificial anisotropic dielectrics as well as the techniques for constructing them have been considered by various authors, and the results are available in the literature[1, 2, 4, 5].

The characteristics of surface waves guided by isotropic dielectric slabs have been studied in great detail and the results are well known[10]. An extension to this problem consists of the study of such waves guided by a uniaxially anisotropic dielectric slab. This latter problem will be considered in Chapter III and it will be found that the surface waves which propagate at a given frequency are finite in number. In addition, it will be shown that the relative dielectric constants of the dielectric tensor must satisfy certain inequalities if surface waves are to propagate.

Another medium which possesses the uniaxial characteristics described above is a plasma in the presence of an infinite, d. c. magnetic field. If a slab of such a plasma, with the optical axis oriented parallel to the slab, is excited by a magnetic line source some very interesting phenomena are observed. These will be discussed in detail in Chapter IV. However, it is interesting to mention some of the results here, and by way of contrast, to mention some of the results obtained by Tamir[11, 12, 13] in the analysis of the source-excited, isotropic plasma slab.

In the case of the uniaxially anisotropic slab it will be shown, for the E-mode case, that an infinite number of surface waves can be supported by the slab at any frequency below the plasma frequency. In addition, the waves are all forward waves. In contrast, Tamir's results show that an isotropic plasma slab can support up to four forward or backward surface waves, and these carry power in opposite directions in the plasma and air regions. Other contrasting results are also found to exist. Above the plasma frequency, in the anisotropic case, it is found that a descrete infinity of nonspectral leaky wave poles exist, only a finite number of which contribute residue terms to the field. In Tamir's problem the nonspectral leaky waves do not occur. Of course, the continuous spectrum associated with open structures occurs in both the isotropic as well as the anisotropic case.

CHAPTER II
FORMULATION OF THE GENERAL EQUATIONS

The representation of electromagnetic fields in cylindrical regions is greatly simplified by expressing the fields in terms of their longitudinal and transverse components with respect to the longitudinal coordinate z. The transverse fields can then be represented in terms of a complete set of vector modes characteristic of the transverse field distribution, and the longitudinal fields can be derived directly from the transverse fields. In this way the problem is reduced to one of solving a set of one-dimensional transmission line equations. The techniques are equally valid for isotropic, as well as uniaxially anisotropic regions.[6,9,19]

The formulation described above will be outlined for a region filled with a medium of permeability μ_o and a relative dyadic permitivity given by

$$\underset{\sim}{\varepsilon} = \varepsilon_2 \underline{x}_o \underline{x}_o + \varepsilon_1 \underline{y}_o \underline{y}_o + \varepsilon_1 \underline{z}_o \underline{z}_o \tag{2-1}$$

for the case where the optical axis coincides with the x axis (o a x), and

$$\underset{\sim}{\varepsilon} = \varepsilon_1 \underline{x}_o \underline{x}_o + \varepsilon_1 \underline{y}_o \underline{y}_o + \varepsilon_2 \underline{z}_o \underline{z}_o, \tag{2-2}$$

for the case where the optical axis coincides with the z axis (o a z). The inhomogeneous Maxwell equations then have the form

$$\nabla \times \underline{E} = - j\omega\mu_o \underline{H} - \underline{M} \tag{2-3}$$

and

$$\nabla \times \underline{H} = j\omega\varepsilon_o \underset{\sim}{\varepsilon} \cdot \underline{E} + \underline{J} \tag{2-4}$$

where $\underline{E}$, $\underline{H}$, $\underline{M}$ and $\underline{J}$ are the electric field, the magnetic field, the magnetic source current density and the electric source current density, respectively. A time dependence $e^{j\omega t}$ is assumed.

The Maxwell equations can be put into the equivalent transverse (to z) form by using the standard techniques outlined in the literature.[9,19] It is pointed out that the results will be given for the two dimensional case (i.e. $\partial/\partial y \equiv 0$), since the problems considered subsequently fall into this category. For the transverse fields $\underline{H}_t$ and $\underline{E}_t$ one readily obtains the following equations:

$$-\frac{\partial \underline{E}_t}{\partial z} = j\omega\mu_o\left[\underline{\underline{1}}_t + \frac{1}{k_o^2 \epsilon_i} \nabla_t \nabla_t\right] \cdot (\underline{H}_t \times \underline{z}_o) + \hat{\underline{M}}_t \times \underline{z}_o \tag{2-5}$$

$$-\frac{\partial \underline{H}_t}{\partial z} = j\omega\epsilon_o\left[\underline{\underline{\epsilon}}_t + \frac{1}{k_o^2} \nabla_t \nabla_t\right] \cdot (\underline{z}_o \times \underline{E}_t) + \underline{z}_o \times \hat{\underline{J}}_t \tag{2-6}$$

where

$$k_o^2 = \omega^2 \mu_o \epsilon_o,$$

$$\epsilon_i = \begin{cases} \epsilon_1 , & (o\ a\ x) \\ \epsilon_2 , & (o\ a\ z) \end{cases}$$

and

$$\underline{\underline{\epsilon}}_t = \begin{cases} \epsilon_1 \underline{x}_o \underline{x}_o + \epsilon_2 \underline{y}_o \underline{y}_o , & (o\ a\ x) \\ \epsilon_1 (\underline{x}_o \underline{x}_o + \underline{y}_o \underline{y}_o) , & (o\ a\ z). \end{cases}$$

The equivalent transverse source currents $\hat{\underline{M}}_t$ and $\hat{\underline{J}}_t$ are given by

$$\hat{\underline{M}}_t = \underline{M}_t - \frac{\nabla_t \times (\underline{z}_o J_z)}{j\omega\epsilon_o \epsilon_i} , \tag{2-7}$$

and

$$\hat{\underline{J}}_t = \underline{J}_t - \frac{\nabla_t \times (\underline{z}_o M_z)}{j\omega\mu_o} . \tag{2-8}$$

The longitudinal field components can then be expressed in terms of the transverse field components. Thus,

$$H_z = \frac{1}{j\omega\mu_o}\left[\nabla_t \cdot (\underline{z}_o \times \underline{E}_t) - M_z\right], \tag{2-9}$$

and

$$E_z = \frac{1}{j\omega\epsilon_o\epsilon_i}\left[\nabla_t \cdot (\underline{H}_t \times \underline{z}_o) - J_z\right]. \tag{2-10}$$

For the problems to be considered the transverse region is unbounded in the trans-

verse direction, so that a radiation condition must be satisfied at infinity. In the z direction the boundary conditions will be specified for the particular geometries considered.

Since the region under consideration is uniform in the z direction, the transverse components of the electric and magnetic fields can be expressed in the form $V(z, \xi)\ \underline{e}\ (x, \xi)$ and $I(z, \xi)\ \underline{h}\ (x, \xi)$, where ξ is the continuous (real) modal wavenumber in the transverse (x) direction. Also, the homogeneous nature of the transverse cross section permits the decomposition of the vector eigenfunction into E and H modes relative to z. This is the same as the representation for the isotropic case. Thus, the transverse fields and source terms are expressed as follows:

$$\underline{E}_t(x, z) = \int_{-\infty}^{\infty} V'(z, \xi)\ \underline{e}'(x, \xi)\ d\xi + \int_{-\infty}^{\infty} V''(z, \xi)\ \underline{e}''(x, \xi) d\xi, \tag{2-11a}$$

$$\underline{H}_t(x, z) = \int_{-\infty}^{\infty} I'(z, \xi)\underline{h}'(x, \xi)\ d\xi + \int_{-\infty}^{\infty} I''(z, \xi)\ \underline{h}''(x, \xi) d\xi, \tag{2-11b}$$

$$\hat{\underline{J}}_t(x, z) = \int_{-\infty}^{\infty} i'(z, \xi)\underline{e}'(x, \xi) d\xi + \int_{-\infty}^{\infty} i''(z, \xi)\underline{e}''(x, \xi) d\xi, \tag{2-11c}$$

$$\hat{\underline{M}}_t(x, z) = \int_{-\infty}^{\infty} v'(z, \xi)\ \underline{h}'(x, \xi) d\xi + \int_{-\infty}^{\infty} v''(z, \xi)\underline{h}''(x, \xi) d\xi, \tag{2-11d}$$

$$\underline{h} = \underline{z}_o \times \underline{e},$$

where the single and double primes denote E and H modes.

Upon substituting equations (2-11) into (2-5) and (2-6), and remembering the facts that for E modes $\underline{e} = e_{x=o}\ \underline{x}$ and for H modes $\underline{h} = h_{x=o}\ \underline{x}$, and the fact that $\underline{e}'$ and $\underline{e}''$ are linearly independent vector functions, one obtains the transmission line equations and associated eigenvalue problems. Thus, for the (o a x) case, the separation procedure yields for a particular E mode

$$-\frac{dV'(z, \xi)}{dz} = j\ \varkappa'_z Z I'(z, \xi) + v'(z, \xi), \tag{2-12a}$$

$$-\frac{dI'(z, \xi)}{dz} = j\ \varkappa'_z Y' V'(z, \xi) + i'(z, \xi), \tag{2-12b}$$

$$\varkappa'_z = \sqrt{\frac{\epsilon_2}{\epsilon_1}}\ \sqrt{k_o^2 \epsilon_1 - \xi^2}\ , \quad Z' = \frac{1}{Y'} = \frac{\varkappa_{z'}}{\omega \epsilon_o \epsilon_2}\ , \tag{2-12c}$$

and

$$\nabla_t \nabla_t \cdot \underline{e}'(x,\xi) = -\xi^2 \underline{e}'(x,\xi), \tag{2-13a}$$

$$\nabla_t \nabla_t \cdot \underline{h}'(x,\xi) = 0. \tag{2-13b}$$

The E modes are usually referred to as extraordinary type modes. By applying the same procedure for a particular H mode one obtains

$$-\frac{dV''(z,\xi)}{dz} = j\kappa''_z Z'' I''(z,\xi) + v''(z,\xi), \tag{2-14a}$$

$$-\frac{dI''(z,\xi)}{dz} = j\kappa''_z Y'' V''(z,\xi) + i''(z,\xi), \tag{2-14b}$$

$$\kappa''_z = \sqrt{k_o^2 \epsilon_1 - \xi^2}, \qquad Z'' = \frac{\omega\mu_o}{\kappa''_z} \tag{2-14c}$$

and

$$\nabla_t \nabla_t \cdot \underline{h}''(x,\xi) = -\xi^2 \underline{h}''(x,\xi) \tag{2-15a}$$

$$\nabla_t \nabla_t \cdot \underline{e}'' = 0 \tag{2-15b}$$

The H modes are referred to as ordinary type modes.

The same procedure outlined above, applied in the (o a z) case yields similar results. Thus for E modes (extraordinary type modes) one obtains

$$-\frac{dV'(z,\xi)}{dz} = j\kappa'_z Z' I'(z,\xi) + v'(z,\xi) \tag{2-16a}$$

$$-\frac{dI'(z,\xi)}{dz} = j\kappa'_z Y' V'(z,\xi) + i'(z,\xi) \tag{2-16b}$$

$$\kappa'_z = \sqrt{\frac{\epsilon_1}{\epsilon_2}}\sqrt{k^2\epsilon_2 - \xi^2}, \quad Z' = \frac{\kappa'_z}{\omega\epsilon_o\epsilon_1} \tag{2-16c}$$

and

$$\nabla_t \nabla_t \cdot \underline{e}'(x,\xi) = -\xi^2 \underline{e}'(x,\xi), \tag{2-17a}$$

$$\nabla_t \nabla_t \cdot \underline{h}'(x,\xi) = 0. \tag{2-17b}$$

For a particular H mode (ordinary type mode) the results are

$$-\frac{dV''(z,\xi)}{dz} = j\kappa''_z Z'' I''(z,\xi) + v''(z,\xi) \tag{2-18a}$$

$$-\frac{dI''(z,\xi)}{dz} = j\kappa''_z Y'' V''(z,\xi) + i''(z,\xi) \tag{2-18b}$$

$$\kappa''_z = \sqrt{k^2\epsilon_1 - \xi^2}\ , \quad Z'' = \frac{\omega\mu_o}{\kappa''_z} \tag{2-18c}$$

and

$$\nabla_t\nabla_t \cdot \underline{h}''(x,\xi) = -\xi^2\underline{h}''(x,\xi) \tag{2-19a}$$

$$\nabla_t\nabla_t \cdot \underline{e}''(x,\xi) = 0. \tag{2-19b}$$

It has been mentioned that the problems to be considered subsequently are charactized by unbounded cross sections in the transverse direction. Hence, equation (2-13a), (2-15a), (2-17a) and (2-19a) must all satisfy the radiation condition at infinity. Appropriate solutions for these equations would then be of the form

$$\underline{e}(x,\xi) = \frac{1}{\sqrt{2\pi}}\, e^{-j\xi x}\, \underline{x}_o \tag{2-20}$$

for E modes, and

$$\underline{h}(x,\xi) = \frac{1}{\sqrt{2\pi}}\, e^{-j\xi x}\, \underline{x}_o \tag{2-21}$$

for H modes.

The vector functions $\underline{e}$ and $\underline{h}$ are chosen to satisfy the usual orthogonality conditions[6], so that the various current, voltage and source amplitude functions are given by the following equations:

$$V(z,\xi) = \int_{-\infty}^{\infty} \underline{E}_t(x,z) \cdot \underline{e}^*(x,\xi)\, dx\ , \tag{2-22a}$$

$$I(z,\xi) = \int_{-\infty}^{\infty} \underline{H}_t(x,z) \cdot \underline{h}^*(x,\xi)\, dx, \tag{2-22b}$$

$$v(z,\xi) = \int_{-\infty}^{\infty} \hat{\underline{M}}_t(x,z) \cdot \underline{h}^*(x,\xi)\, dx, \tag{2-22c}$$

$$i(z,\xi) = \int_{-\infty}^{\infty} \hat{\underline{J}}_t(x,z) \cdot \underline{e}^*(x,\xi)\, dx, \tag{2-22d}$$

where* denotes complex conjugate.

Although the preceding formulation has been outlined for two dimensional uniaxially anisotropic regions, the problems to be considered will also involve isotropic regions. Hence, the modal formulation for such regions[9] will also be utilized in subsequent work.

CHAPTER III

SURFACE WAVES GUIDED BY A UNIAXIALLY ANISOTROPIC DIELECTRIC SLAB

In this chapter the properties of surface waves guided by a uniaxially anisotric dielectric slab will be studied, with the analysis being limited to the source free case. The propagation of surface waves in a slab of dielectric (isotropic or anisotropic) depends upon the phenomenon of total reflection at the inner boundaries of the slab. It is well known that when total reflection takes place at a dielectric interface the propagation constant in the direction perpendicular to the interface and outside the dielectric becomes purely imaginary. The fields outside the dielectric then decay exponentially with distance from the interface.

The geometry of the problem to be considered is illustrated in Fig. 3.1. The slab consists of an anisotropic dielectric with dielectric tensor given by equation (2-1) or (2-2), and with ε_1 and ε_2 real and positive. The medium which surrounds the slab on either side is isotropic with a relative dielectric constant ε. Because of the obvious symmetry of the problem

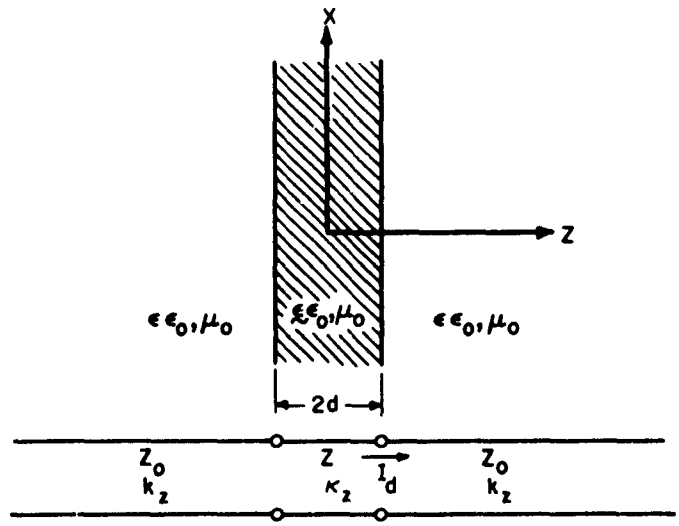

Fig. 3.1: Anisotropic dielectric slab and equivalent transmission line.

two bisections will be considered, a short circuit or electric wall (s b), and an open circuit or magnetic wall (o b). The analysis will be limited to the study of E modes since the properties of H modes (ordinary modes) in the slab are the same as those of waves propagating in an isotropic region.

1. The Transverse Resonance Solution

It will be convenient to anticipate the fact that the surface wave resonances are finite in number at any given frequency. Hence, the subscript m will be introduced on all subsequent results to denote a particular surface wave. The wavenumbers inside and outside the slab in the x direction are denoted, respectively, by $\varkappa_{xm}$ and k_{xm}. These must be equal for the boundary conditions to be matched at the interface. The characteristic impedance of the equivalent transmission line is given by

$$Z_m = \begin{cases} \dfrac{\varkappa_{zm}}{\omega\epsilon_o\epsilon_2} \quad , \quad (o \text{ a } x) \quad , & (3\text{-}1a) \\ \dfrac{\varkappa_{zm}}{\omega\epsilon_o\epsilon_1} \quad , \quad (o \text{ a } z) \quad , & (3\text{-}1b) \end{cases}$$

for $|z| \leq d$, and

$$Z_{om} = \frac{k_z}{\omega\epsilon_o\epsilon} \quad , \tag{3-2}$$

for $|z| > d$. $\varkappa_z m$ and $k_z m$ are the wave numbers in the z direction, inside and outside the slab respectively.

The values of $\varkappa_{xm}$, $\varkappa_{zm}$, and k_{zm} for the surface waves which will propagate are obtained by solving simultaneously the transverse resonance equation and the dispersion relation. This latter relation is obtained from equations (2-12c) and (2-16c) for the region $|z| \leq d$. For the present problem, the dispersion relation within the slab is written as follows:

$$k_o^2 \epsilon_1 \epsilon_2 = \begin{cases} \varkappa_{xm}^2 \epsilon_2 + \varkappa_{zm}^2 \epsilon_1 \quad , \quad (o \text{ a } x), & (3\text{-}3a) \\ \varkappa_{xm}^2 \epsilon_1 + \varkappa_{zm}^2 \epsilon_2 \quad , \quad (o \text{ a } z). & (3\text{-}3b) \end{cases}$$

For the region $|z| > d$, the dispersion relation is given by

$$k_o^2 \epsilon = \varkappa_{xm}^2 + k_{zm}^2 \, . \tag{3-4}$$

The transverse resonance equation for either bisection is given by

$$\overleftarrow{Z}(d) + \overrightarrow{Z}(d) = 0,$$

Where $\overleftarrow{Z}(d)$ is the impedance looking to the left at z = d and $\overrightarrow{Z}(d)$ is the impedance looking to the right at z = d. Thus, for short circuit or open circuit bisections taken at z = 0 in Fig. 3.1, one obtains the following equations:

s b case

$$j\frac{\varkappa_{zm}}{\epsilon_2}\tan\varkappa_{zm}d + \frac{k_{zm}}{\epsilon} = 0, \text{ (o a x)} \quad (3\text{-}5a)$$

$$j\frac{\varkappa_{zm}}{\epsilon_1}\tan\varkappa_{zm}d + \frac{k_{zm}}{\epsilon} = 0, \text{ (o a z)} \quad (3\text{-}5b)$$

o b case

$$-j\frac{\varkappa_{zm}}{\epsilon_2}\cot\varkappa_{zm}d + \frac{k_{zm}}{\epsilon} = 0, \text{ (o a x)} \quad (3\text{-}6a)$$

$$-j\frac{\varkappa_{zm}}{\epsilon_2}\cot\varkappa_{zm}d + \frac{\varkappa_{zm}}{\epsilon} = 0, \text{ (o a z)} \quad (3\text{-}6b)$$

A necessary condition for the propagation of surface waves within the slab is that the propagation constant in the z direction in the outer medium be purely imaginary, that is

$$k_{zm} = -j\left|k_{zm}\right|.$$

With this last result, equations (3-3) and (3-4) can be combined to yield

$$k_o^2\,\epsilon_2(\epsilon_1 - \epsilon) = \varkappa_{zm}^2\,\epsilon_1 + \left|k_{zm}\right|^2\epsilon_2, \quad (3\text{-}7)$$

for the (o a x) case, and

$$k_o^2\,\epsilon_1(\epsilon_2 - \epsilon) = \varkappa_{zm}^2\,\epsilon_2 + \left|k_{zm}\right|^2\epsilon_1, \quad (3\text{-}8)$$

for the (o a z) case. Now, introducing the change of variables

$$p = \varkappa_{zm}d \quad (3\text{-}9)$$

and

$$q = \begin{cases} \left|k_{zm}\right| d\sqrt{\dfrac{\epsilon_2}{\epsilon_1}}, & \text{(o a x)}, \\ \left|k_{zm}\right| d\sqrt{\dfrac{\epsilon_1}{\epsilon_2}}, & \text{(o a z)}, \end{cases} \quad (3\text{-}10)$$

equations (3-7) and (3-8) both take the form

$$p^2 + q^2 = a^2 \quad (3\text{-}11)$$

where

$$a^2 = \begin{cases} (k_o d)^2 \frac{\epsilon_2}{\epsilon_1} (\epsilon_1 - \epsilon) \quad , \quad (o\ a\ x), & (3\text{-}12a) \\ (k_o d)^2 \frac{\epsilon_1}{\epsilon_2} (\epsilon_2 - \epsilon) \quad , \quad (o\ a\ z). & (3\text{-}12b) \end{cases}$$

Under the same change of variables (3-9) and (3-10), equations (3-5) and (3-6) become

$$q = \begin{cases} \frac{\epsilon}{\sqrt{\epsilon_1 \epsilon_2}} p \tan p \quad , \quad (s\ b), & (3\text{-}13a) \\ \frac{-\epsilon}{\sqrt{\epsilon_1 \epsilon_2}} p \cot p \quad , \quad (o\ b). & (3\text{-}13b) \end{cases}$$

Note that equation (3-13) is valid for both the (o a x) case and the (o a z) case.

Equation (3-11) is the equation of a circle and it is to be solved simultaneously with equation (3-13). The graphical technique for the solution is illustrated in Fig. 3.2.

The cutoff frequencies for the various surface waves occur when κ_{xm} approaches $k_o^2 \epsilon$, in which case it follows from equations (3-4) and

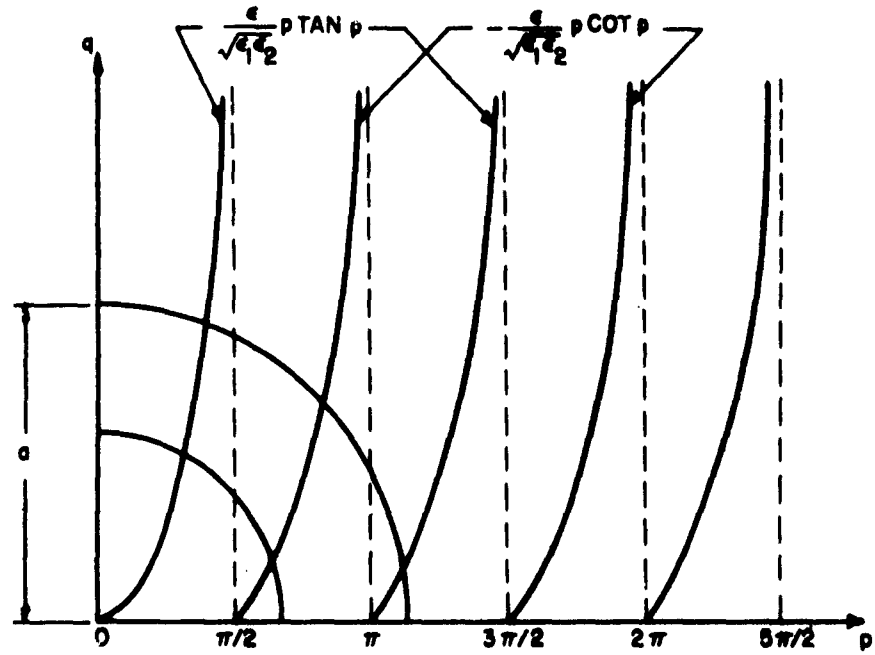

Fig. 3.2: Illustration of the graphical technique for the transverse resonance solution.

(3-10) that q = 0. To satisfy these conditions the relations

$$\tan p = 0 \qquad \cot p = 0$$

must hold in the (s b) and (o b) case respectively. The last equations are satisfied when

$$p = \varkappa_{zm} d = a = \frac{m\pi}{2} , \tag{3-14}$$

where m = 0, 1, 2, ... Note that m is even for the (s b) case and odd for the (o b) case. The cutoff frequencies and wavelengths can be obtained from equations (3-12) and (3-14). When the optical axis coincides with the x axis one obtains

$$f_{cm} = \frac{mc}{4d}\sqrt{\frac{\varepsilon_1}{\varepsilon_2(\varepsilon_1 - \varepsilon)}} , \tag{3-15}$$

and

$$\lambda_{cm} = \frac{4d}{m}\sqrt{\frac{\varepsilon_2}{\varepsilon_1}(\varepsilon_1 - \varepsilon)} , \tag{3-16}$$

where c is the speed of light in free space. When the optical axis coincides with the z axis the results are

$$f_{cm} = \frac{mc}{4d}\sqrt{\frac{\varepsilon_2}{\varepsilon_1(\varepsilon_2 - \varepsilon)}} , \tag{3-17}$$

and

$$\lambda_{cm} = \frac{4d}{m}\sqrt{\frac{\varepsilon_1}{\varepsilon_2}(\varepsilon_2 - \varepsilon)} . \tag{3-18}$$

It should be pointed out that the lowest cutoff frequency is zero in the case of the short circuit bisection.

Some important facts can now be obtained by interpreting some of the above results. Reference to equation (3-12) shows that when the optical axis coincides with the x axis no surface waves can propagate if $\varepsilon_1 \leq \varepsilon$. Likewise, when the dielectric is anisotropic in the z direction, no surface waves will propagate if $\varepsilon_2 \leq \varepsilon$.

2. The Dispersion Curves

An overall picture of the behavior of the surface waves can be obtained from an examination of the dispersion curves given by λ/λ_x vs. λ/d. λ_x is the wavelength in the x direction. In order to obtain the dispersion curves it will be necessary to obtain an expression for λ/λ_x in terms of p and q. This expression, together with a knowledge of the behavior of the roots of the transverse resonance equation (see Fig. 3.2), enables one to plot λ/λ_x vs. λ/d.

Equations (3-3) and (3-4) can be written, with the aid of (3-10), as follows:

(o a x) case

$$p^2\varepsilon = (k_o d)^2 \varepsilon_2\varepsilon - (\varkappa_{xm} d)^2 \frac{\varepsilon_2\varepsilon}{\varepsilon_1} , \tag{3-19a}$$

(o a z) case

$$p^2\varepsilon = k_o^2 \varepsilon_1\varepsilon - (\varkappa_{xm} d)^2 \frac{\varepsilon_1\varepsilon}{\varepsilon_2} , \tag{3-19b}$$

$$q^2 \epsilon_1 = -(k_o d)^2 \epsilon_2 \epsilon + (\varkappa_{xm} d)^2 \epsilon_2, \quad (3\text{-}20a) \qquad q^2 \epsilon_2 = -k_o^2 \epsilon_1 \epsilon + (\varkappa_{xm} d)^2 \epsilon_1. \quad (3\text{-}20b)$$

Now, combining equations (3-19) and (3-20) solving for $\varkappa_{xm}$, dividing by k_o, and using equations (3-11) and (3-12), one obtains

(o a x) case

$$\frac{\lambda}{\lambda_x} = \sqrt{\frac{\epsilon^2 p + \epsilon_1 q^2}{p^2 + q^2}}, \quad (3\text{-}21a)$$

(o a z) case

$$\frac{\lambda}{\lambda_x} = \sqrt{\frac{\epsilon^2 p + \epsilon_2 q^2}{p^2 + q^2}}. \quad (3\text{-}21b)$$

Equations (3-21) can now be used to obtain the qualitative curves shown in Fig. 3.3. It is seen, from Fig. 3.2, that for a infinite, q becomes infinite and p approaches some multiple of $\pi/2$, for a particular surface wave resonance. Hence all the curves intersect

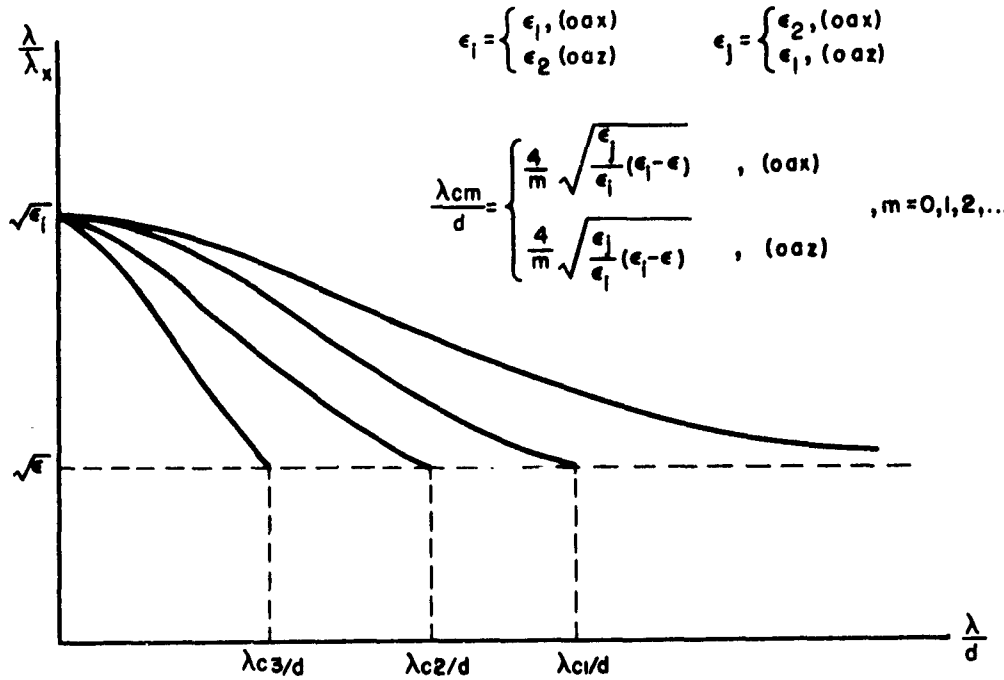

Fig. 3.3: Dispersion curves for the surface waves.

the λ/λ_x axis at $\sqrt{\epsilon_1}$, where ϵ_1 is defined in Fig. 3.3. The lowest surface wave resonance (m = 0) has an asymptotic value of $\lambda/\lambda_x = \sqrt{\epsilon}$ as a approaches zero. This fact can be obtained from equations (3-13a) and (3-21a). The higher order resonances

have curves which end on the line $\lambda/\lambda_x = \sqrt{\varepsilon}$ at values of λ/d given by equations (3-16) and (3-18).

The slope of the curves is Fig. 3.3 is always negative and consequently the surface waves are all forward waves in the x direction. It is expected, then, that the net transfer of power is in the positive x direction. This is actually the case since the only real component of the Poynting vector is $P_x = -E_z H_y^*$ (see equations (3-26) and (3-27) in section 3).

3. The Spatial Variation of the Fields

It is a simple matter to derive the field expressions for the surface waves. These can be expressed directly in terms of the current function which satisfies the equivalent transmission line in Fig. 3.1. It will only be necessary to obtain an expression for the y-component of the magnetic field H_y, the electric field being given by

$$E_x = \begin{cases} -\dfrac{1}{j\omega\varepsilon_o\varepsilon_2}\dfrac{\partial H_y}{\partial z}, & (\text{o a x}) \\ & , \ |z| < d, \\ -\dfrac{1}{j\omega\varepsilon_o\varepsilon_1}\dfrac{\partial H_y}{\partial z}, & (\text{o a z}) \end{cases} \qquad (3\text{-}22a)\ (3\text{-}22b)$$

$$E_z = \begin{cases} \dfrac{1}{j\omega\varepsilon_o\varepsilon_1}\dfrac{\partial H_y}{\partial x}, & (\text{o a x}) \\ & , \ |z| < d, \\ \dfrac{1}{j\omega\varepsilon_o\varepsilon_2}\dfrac{\partial H_y}{\partial x}, & (\text{o a z}) \end{cases} \qquad (3\text{-}23a)\ (3\text{-}23b)$$

$$E_x = -\frac{1}{j\omega\varepsilon_o\varepsilon}\frac{\partial H_y}{\partial z}, \quad |z| > d, \qquad (3\text{-}24)$$

$$E_z = \frac{1}{j\omega\varepsilon_o\varepsilon}\frac{\partial H_y}{\partial x}, \quad |z| > d. \qquad (3\text{-}25)$$

If the amplitude of the current function at z = d is specified as I_d, and if one keeps in mind the continuity requirement for E_x and H_y at the slab interface, then, with the aid of equations (3-22) to (3-25), the following field distributions are obtained:

s b case

(a) $0 \leq z < d$

$$E_x = \frac{I_d}{\sqrt{2\pi}} \frac{\varkappa_{zm}}{j\omega\varepsilon_o\varepsilon_j} e^{-j\varkappa_{xm}x} \frac{\sin \varkappa_{zm} z}{\cos \varkappa_{zm} d} ,$$

$$H_y = \frac{I_d}{\sqrt{2\pi}} e^{-j\varkappa_{xm}x} \frac{\cos \varkappa_{zm} z}{\cos \varkappa_{zm} d} , \qquad (3\text{-}26a)$$

$$E_z = -\frac{I_d}{\sqrt{2\pi}} \frac{\varkappa_{xm}}{\omega \varepsilon_o \varepsilon_i} e^{-j\varkappa_{xm}x} \frac{\cos \varkappa_{zm} z}{\cos \varkappa_{zm} d} ,$$

where $$\varepsilon_i = \begin{cases} \varepsilon_1 , & (o \text{ a } x) \\ \varepsilon_2 , & (o \text{ a } z) \end{cases} \qquad \varepsilon_j = \begin{cases} \varepsilon_2 , & (o \text{ a } x) \\ \varepsilon_1 , & (o \text{ a } z) , \end{cases}$$

(b) $z > d$

$$E_x = \frac{I_d}{\sqrt{2\pi}} \frac{\varkappa_{zm}}{j\omega\varepsilon_o\varepsilon_j} \frac{\sin \varkappa_{zm} d}{\cos \varkappa_{zm} 1} e^{-j\varkappa_{xm}x} e^{-|k_{zm}|(z-d)},$$

$$H_y = \frac{I_d}{\sqrt{2\pi}} e^{-j\varkappa_{xm}x} e^{-|k_{zm}|(z-d)}, \qquad (3\text{-}26b)$$

$$E_z = -\frac{I_d}{\sqrt{2\pi}} \frac{\varkappa_{xm}}{\omega \varepsilon_o \varepsilon} e^{-j\varkappa_{xm}x} e^{-|k_{zm}|(z-d)},$$

o b case

(a) $0 \leq z < d$

$$E_x = -\frac{I_d}{\sqrt{2\pi}} \frac{\varkappa_{zm}}{j\omega\varepsilon_o\varepsilon_j} e^{-j\varkappa_{xm}x} \frac{\cos \varkappa_{zm} z}{\sin \varkappa_{zm} d} ,$$

$$H_y = \frac{I_d}{\sqrt{2\pi}} e^{-j\varkappa_{xm}x} \frac{\sin \varkappa_{zm} z}{\sin \varkappa_{zm} d} , \qquad (3\text{-}27a)$$

$$E_z = -\frac{I_d}{\sqrt{2\pi}} \frac{\varkappa_{xm}}{\omega\varepsilon_o\varepsilon_i} e^{-j\varkappa_{xm}x} \frac{\sin \varkappa_{zm} z}{\sin \varkappa_{zm} d} ,$$

(b) $z > d$

$$E_x = -\frac{I_d}{\sqrt{2\pi}} \frac{\kappa_{zm}}{j\omega\epsilon_o\epsilon_j} \frac{\cos \kappa_{zm} d}{\sin \kappa_{zm} d} e^{-j\kappa_{xm} x} e^{-|k_{zm}|(z-d)},$$

$$H_y = \frac{I_d}{\sqrt{2\pi}} e^{-j\kappa_{xm} x} e^{-|k_{zm}|(z-d)}, \qquad (3\text{-}27b)$$

$$E_z = -\frac{I_d}{\sqrt{2\pi}} \frac{\kappa_{xm}}{\omega\epsilon_o\epsilon} e^{-j\kappa_{xm} x} e^{-|k_{zm}|(z-d)}.$$

Equations (3-26) and (3-27) show that the spatial variation of the fields is sinusoidal within the slab and exponentially decaying outside the slab. Furthermore, it can be seen from Fig. 3.2 that as frequency increases for a given surface wave the wave becomes more tightly bound to the slab. Fig. 3.4 shows the spatial variation with z of H_y for the m=0 surface wave. The field distribution is shown for a low frequency as well as for a high frequency.

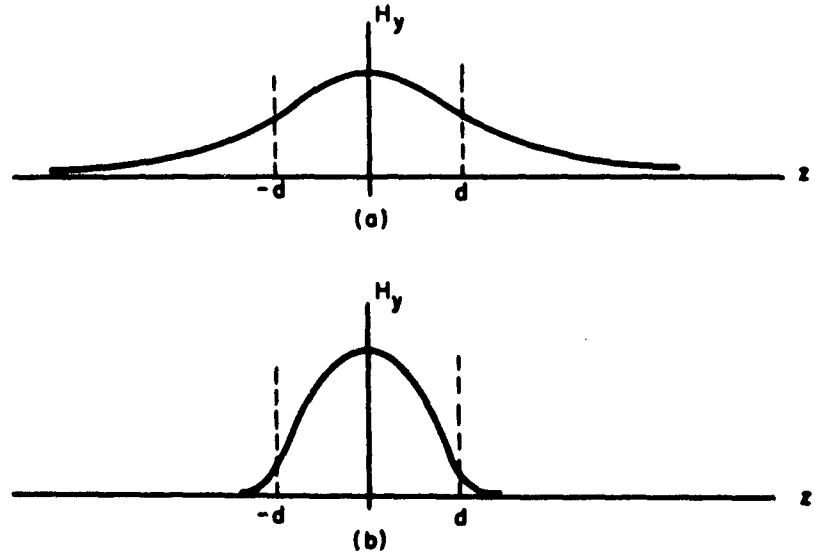

Fig. 3.4: Spatial variation of H_y for the m = 0 resonance, (a) low frequency, (b) high frequency.

CHAPTER IV

THE ELECTROMAGNETIC FIELD OF A UNIAXIALLY ANISOTROPIC PLASMA SLAB EXCITED BY A MAGNETIC LINE SOURCE

The problem to be considered next consists of an analysis of the properties of the electromagnetic field of a uniaxially anisotropic plasma slab excited by a magnetic line source. The slab is infinite and planar with a thickness 2d and bounded on both sides by free space. The infinite magnetic field is applied parallel to the slab so that the optical axis coincides with the x axis. Maxwell's equations for the situation described are given by equations (2-3) and (2-4) with $\underline{J} = 0$ and $\underline{M} = \delta(x)\,\delta(z - b)\,\underline{y}_o$. It is seen that the direction of the magnetic line source is chosen perpendicular to the optical axis. The dielectric properties of the plasma are given by the relative dielectric tensor

$$\underline{\underline{\epsilon}} = \epsilon_p \underline{x}_o \underline{x}_o + \underline{y}_o \underline{y}_o + \underline{z}_o \underline{z}_o \tag{4-1}$$

where

$$\epsilon_p = 1 - \left(\frac{\omega_p}{\omega}\right)^2 \tag{4-2}$$

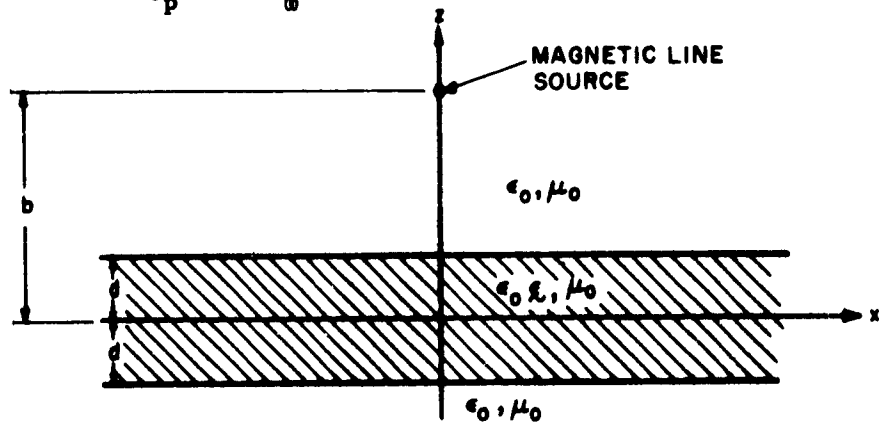

Fig. 4.1: Geometry of the source excited plasma slab.

and ω_p is the plasma frequency. The geometry of the problem described above is illustrated in Fig. 4.1. Two cases will actually be considered, one where the source is outside the slab and the other where the source is located at z = 0 in the form of a slot in a ground plane.

1. The Formal Solution

a: The magnetic line source is located outside the slab.

It follows readily from Maxwell's equations that, for the configuration in

Fig. 4.1, the magnetic field will have only a y component and the electric field will have only x and z components. Hence, only E-modes with respect to the z direction will be of interest. The symmetry of the geometry warrants the simultaneous consideration of the usual short circuit and open circuit bisections of the equivalent transmission line network. This is illustrated in Fig. 4.2. The propagation factor

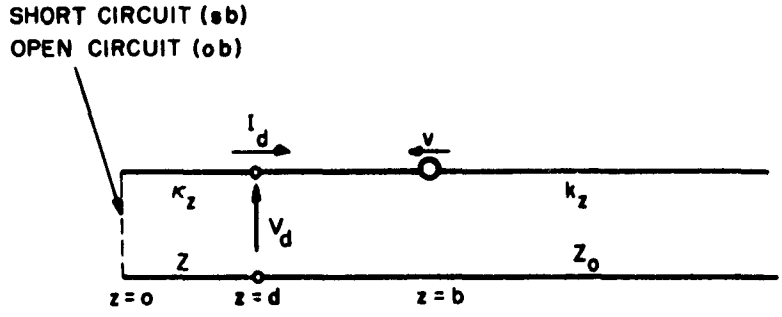

Fig. 4.2: Equivalent transmission line network for the geometry of Fig. 4.1.

and characteristic impedance of the equivalent transmission line in the region $0 \leq z < d$ are obtained from equations (2-12c) with $\epsilon_1 = 1$ and $\epsilon_2 = \epsilon_p$. Thus,

$$\kappa_z = \sqrt{\epsilon_p}\ \sqrt{k_o^2 - \xi^2}\ , \tag{4-3}$$

and

$$Z = \frac{1}{Y} = \frac{\kappa_z}{\omega \epsilon_o \epsilon_p}\ , \tag{4-4}$$

where ξ is the wavenumber in the x direction. For $z > d$, the corresponding parameters are

$$k_z = \sqrt{k_o^2 - \xi^2}\ , \tag{4-5}$$

and

$$Z_o = \frac{1}{Y_o} = \frac{k_z}{\omega \epsilon_o}\ . \tag{4-6}$$

The magnitude of the voltage generator in Fig. 4.2 is obtained from equation (2-22c). Thus, with

$$\underline{h}(x, \xi) = \frac{1}{\sqrt{2\pi}}\ e^{-j\xi x}\ \underline{Y}_o\ ,$$

one obtains

$$v(z, \xi) = \frac{1}{\sqrt{2\pi}}\ \delta(z - b).$$

The magnetic field H_y is most readily expressed in terms of the current function which satisfies the transmission line in Fig. 4.2. The x and z components of the electric field are then readily derived as derivatives of H_y. These results can then be expressed as follows:

$$H_y = \frac{1}{\sqrt{2\pi}} \int_{-\infty}^{\infty} I(z, \xi)\, e^{-j\xi x}\, d\xi \quad , \tag{4-7}$$

and

$$E_x = -\frac{1}{j\omega\epsilon_o\epsilon_p} \frac{\partial H_y}{\partial z} \quad , \quad 0 \leq z < d, \tag{4-8a}$$

$$E_x = -\frac{1}{j\omega\epsilon_o} \frac{\partial H_y}{\partial z} \quad , \quad d < z < \infty , \tag{4-8b}$$

$$E_z = \frac{1}{j\omega\epsilon_o} \frac{\partial H_y}{\partial x} \quad , \quad 0 < z < \infty . \tag{4-8c}$$

The solution for the transverse current function is readi y obtained[9] and is given by

$$I(z, \xi) = \begin{cases} -\frac{1}{\sqrt{2\pi}} \frac{e^{-jkz(b-d)}}{\overleftrightarrow{Z}(d)} \frac{\cos \varkappa_z z}{\cos \varkappa_z d} \quad , \text{(s b)}, & (4\text{-}9a) \\ -\frac{1}{\sqrt{2\pi}} \frac{e^{-jkz(b-d)}}{\overleftrightarrow{Z}(d)} \frac{\sin \varkappa_z z}{\sin \varkappa_z d} \quad , \text{(o b)}, & (4\text{-}9b) \end{cases}$$

for $0 \leq z < d$, and

$$I(z, \xi) = -\frac{\omega\epsilon_o}{2\sqrt{2\pi}\, k_z} \left[e^{-jk_z|z-b|} - \overleftrightarrow{\Gamma}(d)\, e^{-jk_z(z+b-2d)} \right], \tag{4-10}$$

for $z > d$, where

$$\overleftrightarrow{Z}(d) = \begin{cases} j\frac{\varkappa_z}{\omega\epsilon_o\epsilon_p} \tan \varkappa_z d + \frac{k_z}{\omega\epsilon_o} \quad , \quad \text{(s b)}, & (4\text{-}11a) \\ -j\frac{\varkappa_z}{\omega\epsilon_o\epsilon_p} \cot \varkappa_z d + \frac{k_z}{\omega\epsilon_o} \quad , \quad \text{(o b)}, & (4\text{-}11b) \end{cases}$$

and

$$\overleftarrow{\Gamma}(d) = \begin{cases} \dfrac{j\frac{1}{\epsilon_p}\varkappa_z \tan \varkappa_z d - k_z}{j\frac{1}{\epsilon_p}\varkappa_z \tan \varkappa_z d + k_z}, & (\text{s b}), \qquad (4\text{-}12a) \\ \dfrac{j\frac{1}{\epsilon_p}\varkappa_z \cot \varkappa_z d + k_z}{j\frac{1}{\epsilon_p}\varkappa_z \cot \varkappa_z d - k_z}, & (\text{o b}). \qquad (4\text{-}12b) \end{cases}$$

b: The magnetic line source is located at z = 0.

When the magnetic line source is located at z = 0 in the form of a slot in a conducting ground plane, the only difference in the equivalent transmission line network in Fig. 4.2 is that the voltage source is located at z = 0. The current function is then given by (remembering that only the (s b) case is of interest)

$$I(z,\xi) = -\frac{\omega \epsilon_o \epsilon_p}{\sqrt{2\pi}}\left[\frac{\frac{1}{\epsilon_p}\varkappa_z \cos \varkappa_z(z-d) - j k_z \sin \varkappa_z (z-d)}{\varkappa_z (k_z \cos \varkappa_z d + j\frac{1}{\epsilon_p}\sin \varkappa_z d)}\right] \qquad (4\text{-}13)$$

for $0 \leq z \leq d$, and

$$I(z,\xi) = -\frac{\omega \epsilon_o \epsilon_p}{\sqrt{2\pi}} \frac{e^{-jk_z(z-d)}}{\epsilon_p k_z \cos \varkappa_z d + j\varkappa_z \sin \varkappa_z d} \qquad (4\text{-}14)$$

for $d \leq z < \infty$.

c: Evaluation of the free space field.

In evaluating the fields, interest will be centered on the region above the slab, so that equations (4-10) and (4-14) will be the functions in the integral given by (4-7). The treatment of the fields within the slab can be handled by the same techniques presented in the subsequent outline, although this will not be carried out here. Tamir[11] has evaluated the fields within the slab for the isotropic plasma and a complete development of the techniques involved can be found in his work. The methods employed in the evaluation of the integral in (4-7) are well known[9,10,11] and will be considered only briefly here.

To insure the convergence of the integral and the satisfaction of the radiation condition, it is required that $\mathrm{Re}k_z > 0$ and $\mathrm{Im}k_z < 0$. The integrand has branch points

at $\xi = \pm k_o$ and the choice of branch cuts which satisfies the necessary conditions is

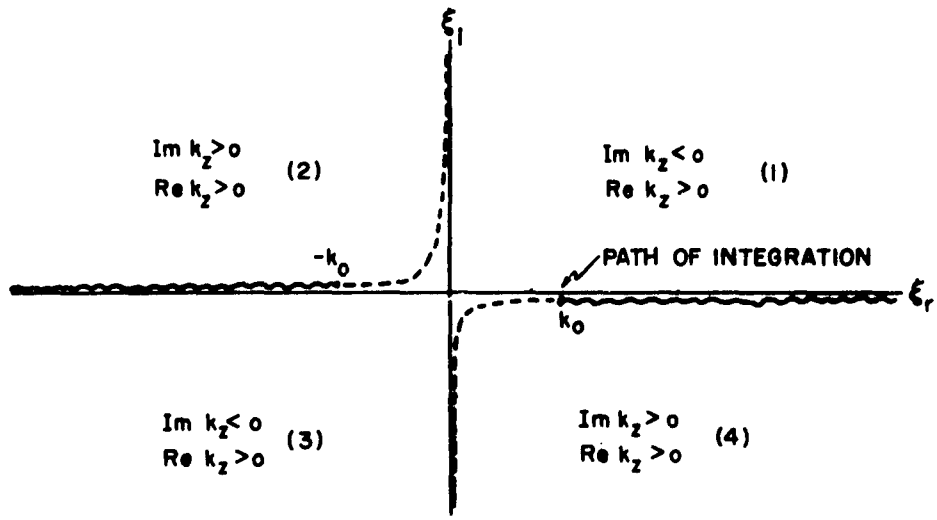

Fig. 4.3: Illustrating the choice of branch cuts in the ξ plane.

illustrated in Fig. 4.3. The situation in Fig. 4.3 is depicted for the case of vanishingly small losses, so that the path of integration is clearly defined.

In order to obtain a steepest descent approximation for the fields it is convenient to put the integral in a more suitable form. This is accomplished by introducing a cylindrical coordinate representation and a change of variable given by the transformation

$$\xi = k_o \sin \varphi \,, \tag{4-15a}$$

$$k_z = k_o \cos \varphi \,, \tag{4-15b}$$

$$\varphi = \varphi_r + j\varphi_i \quad . \tag{4-15c}$$

The cylindrical coordinate system for the line source outside the plasma slab is illustrated in Fig. 4.4, while the geometry for the source located at z = 0 is illustrated in Fig. 4.5. In the former case the change to cylindrical coordinates is accomplished by the transformation

$$x = r \sin \theta \quad , \tag{4-16a}$$

$$z + b - 2d = r \cos \theta \quad , \tag{4-16b}$$

while in the latter case the required transformation is given by

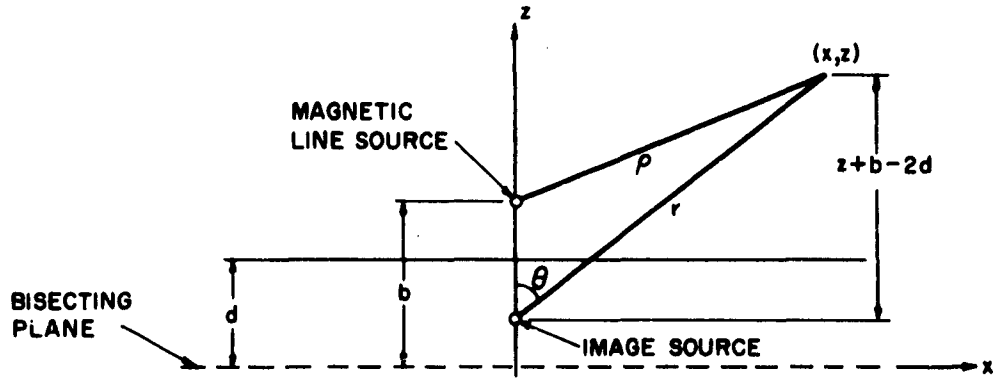

Fig. 4.4: Cylindrical coordinates for source outside the slab.

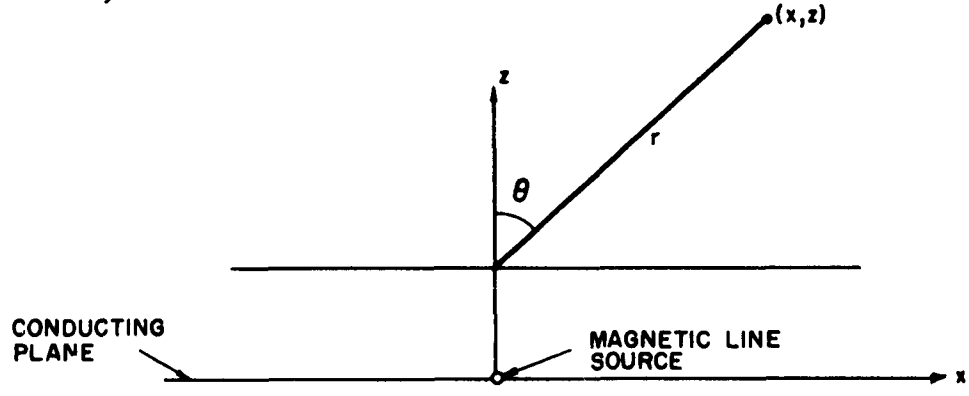

Fig. 4.5: Cylindrical coordinates for source located at z = 0.

$$x = r \sin\theta , \tag{4-17a}$$

$$z - d = r \cos\theta . \tag{4-17b}$$

The integrals which represent the magnetic field above the slab can then be written as

$$H_y = -\frac{\omega \epsilon_o}{4\pi}\left[\pi H_o^{(2)}(k_o p) - \int_p \overleftarrow{\Gamma}(\varphi)\, e^{-jk_o r \cos(\varphi - \theta)}\, d\varphi\right] \tag{4-18}$$

for the case where the line source is located above the slab, and

$$H_y = -\frac{\omega \epsilon_o \epsilon_p}{2\pi} \int_p \frac{e^{-jkr\cos(\varpi - \theta)}}{\epsilon_p \cos(\sqrt{\epsilon_p}\, k_o d \cos\varphi) + j\sqrt{\epsilon_p}\sin(\sqrt{\epsilon_p}\, kd\cos\varphi)}\, d\varphi \tag{4-19}$$

for the magnetic line source located at z = 0. The path of integration in the φ plane is indicated as p. The transformation given in equation (4-15) maps the two sheeted ξ - plane into a connected strip in the φ - plane. The result is indicated in Fig. 4.6, with the numbers indicating those quadrants in the ξ plane which map into the corresponding strips in the φ plane.

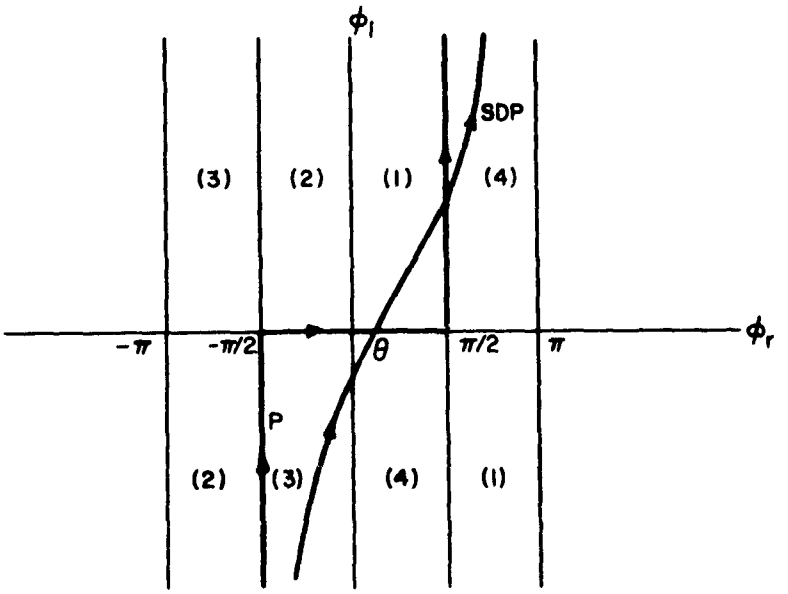

Fig. 4.6: Paths of integration in the φ - plane.

The integrals in equations (4-18) and (4-19) have saddle points at $\varphi = \theta$, so that a steepest descent procedure is used to obtain asymptotic expressions for the magnetic field. The steepest descent path (S D P) is given by

$$\cos(\varphi_r - \theta)\cosh\varphi_i = 1. \tag{4-20}$$

With the line source located outside the slab the magnetic field is given asymptotically by

$$H_y \sim -\frac{\omega\epsilon_o}{4\pi}\left[\pi H_o^{(2)}(k_o\rho) - \sqrt{\frac{2\pi}{k_o r}}\,\overleftarrow{\Gamma}(\theta)\, e^{-j(k_o r - \pi/4)}\right] \tag{4-21}$$

where

$$\overleftarrow{\Gamma}(\theta) = \begin{cases} \dfrac{j \tan (kd\sqrt{\epsilon_p} \cos\theta) - \sqrt{\epsilon_p}}{j \tan (kd\sqrt{\epsilon_p} \cos\theta) + \sqrt{\epsilon_p}}, & \text{(s b)}, \qquad (4\text{-}22a) \\ \dfrac{j \cot (kd\sqrt{\epsilon_p} \cos\theta) + \sqrt{\epsilon_p}}{j \cot (kd\sqrt{\epsilon_p} \cos\theta) - \sqrt{\epsilon_p}}, & \text{(o b)}. \qquad (4\text{-}22b) \end{cases}$$

In addition to the assymptotic term given in equation (4-20) the field also contains residue terms due to poles which are located between the original path of integration P and the steepest descent path (S D P). A typical residue term is given by

$$H_{yp} = \frac{\omega \epsilon_o}{4\pi} \left[2\pi j \left(\frac{N(\varphi)}{\frac{d}{d\varphi} D(\varphi)} \right) e^{-jk_o r \cos(\varphi - \theta)} \right]_{\varphi = \varphi_p} \qquad (4\text{-}23)$$

where $N(\varphi)$ and $D(\varphi)$ are the numerator and denominator of $\overleftarrow{\Gamma}(\varphi)$ respectively. When equation (4-23) is evaluated the result is

$$H_{yp} = \frac{1}{d}\left(\frac{\omega}{\omega_p}\right)^2 \frac{c\epsilon_o}{\sin\varphi_p} e^{-jk_o r \cos(\varphi_p - \theta)}. \qquad (4\text{-}24)$$

When the line source is located at z = 0 the asymptotic evaluation of equation (4-19) yields

$$H_y \sim \omega\epsilon_o\epsilon_p \left[\frac{1}{\epsilon_p \cos(\sqrt{\epsilon_p}\, k_o d \cos\theta) + j\sqrt{\epsilon_p} \sin(\sqrt{\epsilon_p}\, k_o d \cos\theta)} \right] \frac{e^{-j(k_o r - \pi/4)}}{\sqrt{2\pi k_o r}}, \qquad (4\text{-}25)$$

while the evaluation for a particular residue term yields the result

$$H_{yp} = -\frac{\epsilon_o c}{d}\left(\frac{\omega}{\omega_p}\right)^2 \frac{\csc\varphi_p}{\cos(\sqrt{\epsilon_p}\, k_o d \cos\varphi_p)} e^{-jk_o r \cos(\varphi_p - \theta)} \qquad (4\text{-}26)$$

It is pointed out that the radiation field given by equation (4-25) is considerably less complicated than the corresponding term given in equation (4-21) for the case where the magnetic line source is located outside the slab.

The expressions obtained above represent the solutions for the free space field. Before investigating the properties of the field it is necessary to study the transverse resonance equation.

2. Solution of the Transverse Resonance Equation

In order to obtain a more quantitative picture of the fields described in the last section it will be necessary to study the behavior of the poles of the various integrands. These poles correspond to the roots of the transverse resonance equation, given by

$$j \frac{1}{\epsilon_p} \varkappa_z \tan \varkappa_z d + k_z = 0 \ , \ (s\ b) \ , \tag{4-27a}$$

and

$$-j \frac{1}{\epsilon_p} \varkappa_z \cot \varkappa_z d + k_z = 0 \ , \ (o\ b) \ , \tag{4-27b}$$

subject to the auxiliary condition

$$\varkappa_z^2 - \epsilon_p k_z^2 = 0 \tag{4-28}$$

obtained from equations (4-3) and (4-5). For convenience, the change of variables

$$p = \varkappa_z d = p_r + j\, p_i$$

$$q = - k_z d = q_r + j q_i$$

is introduced. Equations (4-27) and (4-28) then take the form

$$q = j \frac{1}{\epsilon_p} p \tan p \quad , \quad (s\ b) \quad , \tag{4-29a}$$

$$q = - j \frac{1}{\epsilon_p} p \cot p \ , \quad (o\ b) \quad , \tag{4-29b}$$

$$p^2 - \epsilon_p q^2 = 0 \ . \tag{4-30}$$

By eliminating q from equations (4-29) and (4-30) one readily obtains the equations

$$1 + \frac{1}{\epsilon_p} \tan^2 p = 0 \quad , \quad (s\ b) \quad , \tag{4-31a}$$

$$1 + \frac{1}{\epsilon_p} \cot^2 p = 0 \quad , \quad (o\ b) \quad . \tag{4-31b}$$

It follows readily from equations (4-31) that p is real only if $\epsilon_p < 0$. However, this fact will fall out as a special case of the subsequent development. By separating the real and imaginary parts of equations (4-31) one readily obtains the results

$$\epsilon_p = \begin{cases} -\dfrac{\sin^2 2p_r - \sinh^2 2p_i}{(\cos 2p_r + \cosh 2p_i)^2}, & (\text{s b}), \quad (4\text{-}32a) \\ -\dfrac{\sin^2 2p_r - \sinh^2 2p_i}{(\cos 2p_r - \cosh 2p_i)^2}, & (\text{o b}), \quad (4\text{-}32b) \end{cases}$$

and

$$\sin 2p_r \sinh 2p_i = 0, \quad (4\text{-}33)$$

for both the (s b) and (o b) cases. Equation (4-33) permits two possible cases, namely either

$$p_i = 0,$$

in which case surface wave resonances exist, or

$$p_r = \frac{n\pi}{2}, \quad n = 0, 1, 2, \ldots$$

in which case leaky wave resonances exist.

In the surface wave case, substitution of $p_i = 0$ in equations (4-32) yields

$$\epsilon_p = \begin{cases} -\tan^2 p_r, & (\text{s b}), \quad (4\text{-}34a) \\ -\cot^2 p_r, & (\text{o b}). \quad (4\text{-}34b) \end{cases}$$

It is seen that the existance of surface waves is possible only when $\epsilon_p < 0$, that is, when the plasma is opaque. For the case where $p_r = n\pi/2$, equations (4-32) yield the result

$$\epsilon_p = \tanh^2 p_i \quad (4\text{-}35)$$

for both bisections, with the stipulation that n is even for the (s b) case and odd for the (o b) case. The above results can be summarized by sketching the loci of the poles in the p-plane with frequency as a parameter. The sketch is shown in Fig. 4.7. It is seen that the surface wave pole loci lie along the p_r axis and the surface wave poles become complex at the plasma frequency. It is also noted that the surface wave poles are infinite in number for any frequency below the plasma frequency.

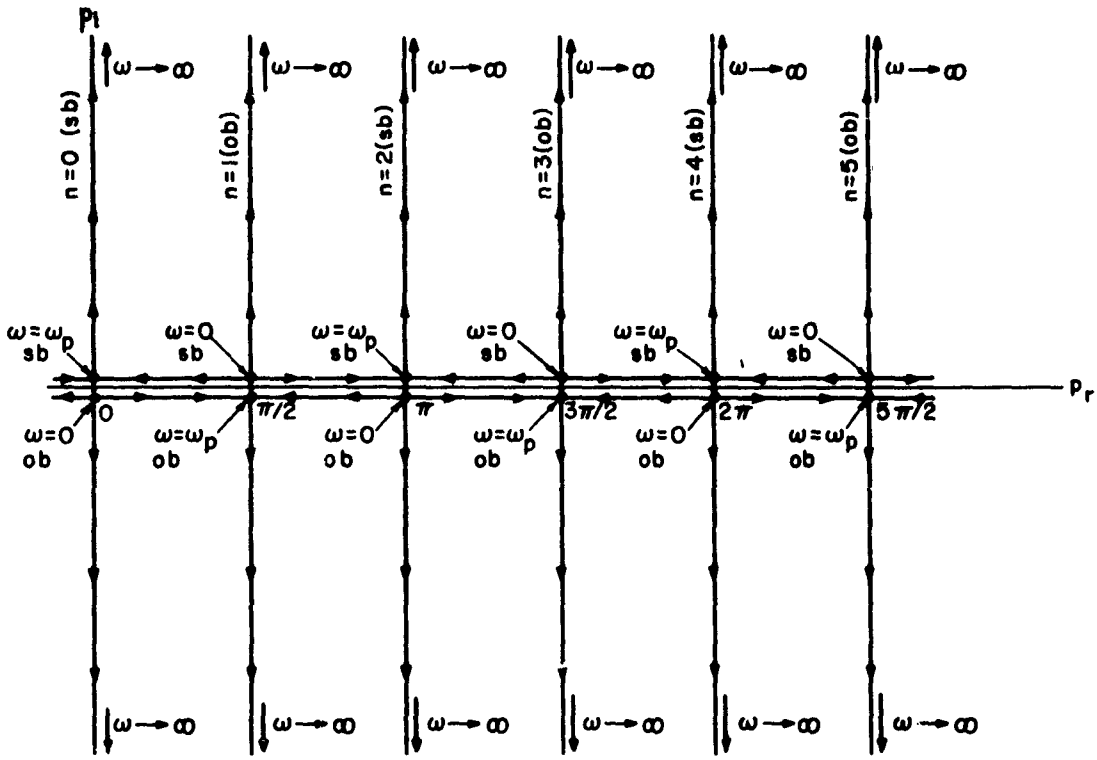

Fig. 4.7: Pole loci in the p-plane. Arrows indicate increasing frequency.

The roots in the q-plane can be obtained from equations (4-29). Thus, in the case of the surface waves with $p = p_r$ and $q = jq_i$ one obtains

$$\epsilon_p q_i = \begin{cases} p_r \tan p_r \quad , \quad (s\,b) \quad , & (4\text{-}36a) \\ -p_r \cot p_r \quad , \quad (o\,b) \quad . & (4\text{-}36b) \end{cases}$$

But from equation (4-30) one can write

$$\epsilon_p q_i = -\frac{p_r^2}{q_i} \quad , \tag{4-37}$$

and hence the result

$$q_i = \begin{cases} -p_r \cot p_r \quad , \quad (s\ b) \quad , & (4\text{-}38a) \\ p_r \tan p_r \quad , \quad (o\ b) \quad , & (4\text{-}38b) \end{cases}$$

is obtained. Equations (4-38) can be used to obtain the surface wave loci shown in Fig. 4.8.

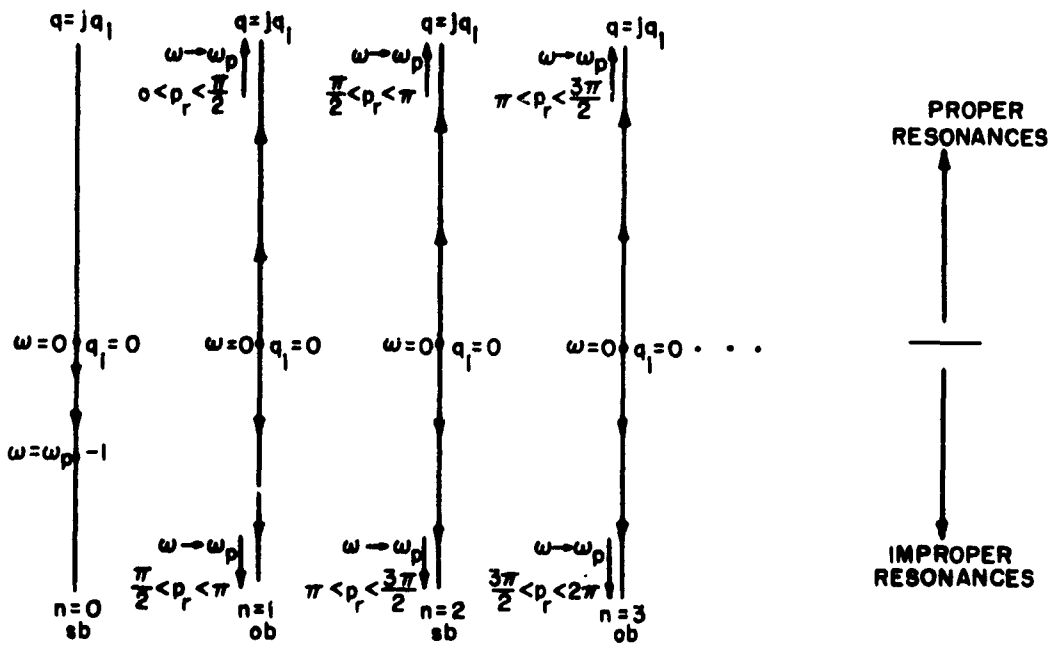

Fig. 4.8: Surface wave pole loci in the q-plane.

In order to obtain the loci of the leaky wave poles in the q-plane, equation (4-35) and the fact that $p_r = n\pi/2$ are substituted into equations (4-29). This last operation yields q as a complex function of frequency (or ϵ_p), and after separating the real and imaginary parts and eliminating the frequency parameter, one obtains for the equation of the leaky wave loci in the q-plane.

$$q_i = -\frac{2q_r}{n\pi} \coth^{-1} \frac{2q_r}{n\pi}, \quad n = 1, 2, 3, \ldots . \qquad (4\text{-}39)$$

The range of values on q_r is given by

$$q_r = \pm \infty, \text{ for } \omega = \omega_p \text{ or } \epsilon_p = 0,$$

and

$$q_r = \pm \frac{n\pi}{2}, \text{ for } \omega = \infty \text{ or } \epsilon_p = 1.$$

For the special case where n = 0, equations (4-29a) and (4-35) yield

$$q_i = - p_i \coth p_i, \tag{4-40}$$

in which case q_i takes on values from -1 to $-\infty$ with increasing frequency. It is pointed out that a pole given by equation (4-40) will not contribute to the field. This fact will become apparent when

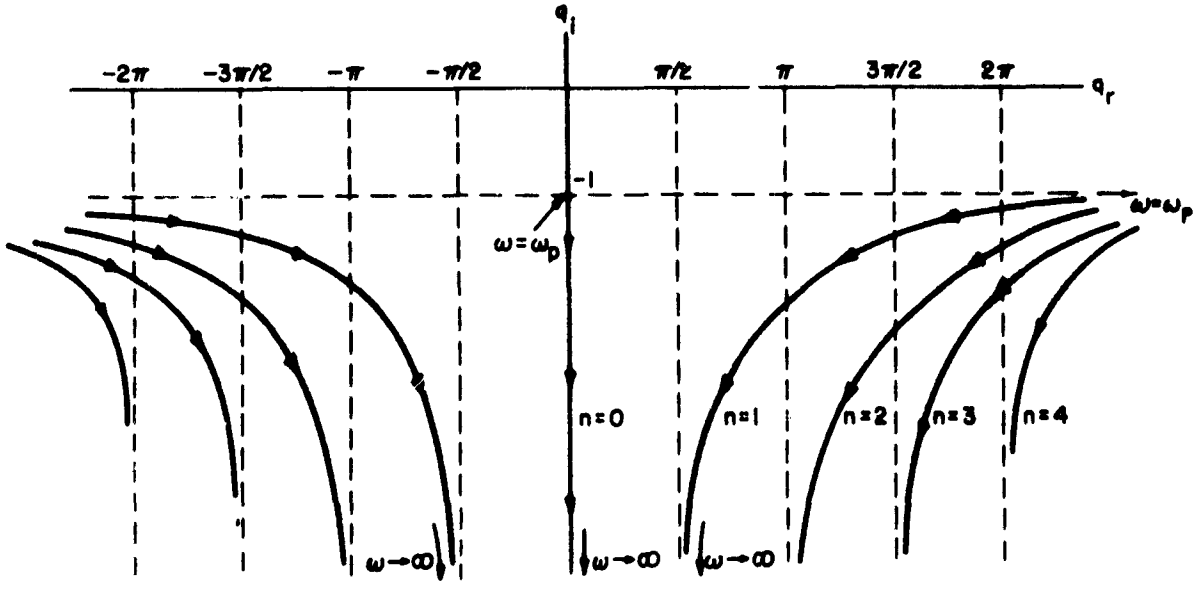

Fig. 4.9: Leaky wave loci in the q-plane.

the pole loci are mapped into the φ plane. The loci of the leaky wave poles are sketched in Fig. 4.9 with the arrows indicating increasing frequency.

The mapping of the pole loci into the φ - plane is accomplished by means of the transformation given by equation (4-15b). Thus, one obtains

$$q = -k_z d = - k_o d \cos \varphi, \tag{4-41}$$

with

$$\varphi = \varphi_r + j\varphi_i .$$

Equation (4-41) is readily separated into the real and imaginary parts to yield

$$q_r = - k_o d \cos \varphi_r \cosh \varphi_i \,, \tag{4-42a}$$

$$q_i = k_o d \sin \varphi_r \sinh \varphi_i \,. \tag{4-42b}$$

The surface wave loci in the q-plane were all located on the imaginary axis and hence it is recognized from equation (4-42a) that these loci will lie on the line $\varphi_r = \pi/2$ in the φ - plane. Equation (4-42b) can then be written as

$$\sinh \varphi_i = \frac{q_i}{k_o d} \,. \tag{4-43}$$

Equation (4-43) can be written, with the aid of equation (4-30), as

$$\sinh^2 \varphi_i = \frac{p_r^2}{\left[\left(\frac{\omega}{c} p_r\right)^2 - \left(\frac{\omega}{c}\right)^2 \right] d} \,, \tag{4-44}$$

where c is the speed of light. Then, considering the n = 0 resonance it is seen that as ω approaches zero, p_r approaches $\pi/2$ and equation (4-44) yields

$$\sinh \varphi_i = - \frac{\pi c}{2 \omega_p d} \,.$$

Also, as ω approaches ω_p, p_r approaches zero and q_i approaches -1, so that equation (4-43) yields

$$\sinh \varphi_i = - \frac{c}{\omega_p d} \,.$$

It is noted that a surface wave pole for the n = 0 case cannot contribute a residue term to the fields. By reasoning similar to the above one can obtain the behavior of the higher surface wave loci in the φ - plane. Thus, for the next three resonances, the following results are obtained:

n = 1,

at $\omega = 0$

$$\sinh \varphi_i = \begin{cases} 0 & \text{(proper resonance)} \\ - \frac{\pi c}{\omega_p d} & \text{(improper resonance),} \end{cases}$$

at $\omega = \omega_p$

$$\sinh \varphi_i = \pm \infty \,;$$

$n = 2$,

at $\omega = 0$

$$\sinh \varphi_i = \begin{cases} \dfrac{\pi c}{2\omega_p d} & \text{(proper resonance)} \\ -\dfrac{3\pi c}{2\omega_p d} & \text{(improper resonance),} \end{cases}$$

at $\omega = \omega_p$

$$\sinh \varphi_i = \pm \infty ;$$

$n = 3$

at $\omega = 0$

$$\sinh \varphi_i = \begin{cases} \dfrac{\pi c}{\omega_p d} & \text{(proper resonance)} \\ -\dfrac{2\pi c}{\omega_p d} & \text{(improper resonance),} \end{cases}$$

at $\omega = \omega_p$

$$\sinh \varphi_i = \pm \infty .$$

The above information for surface wave poles is summarized in Fig. 4.10.

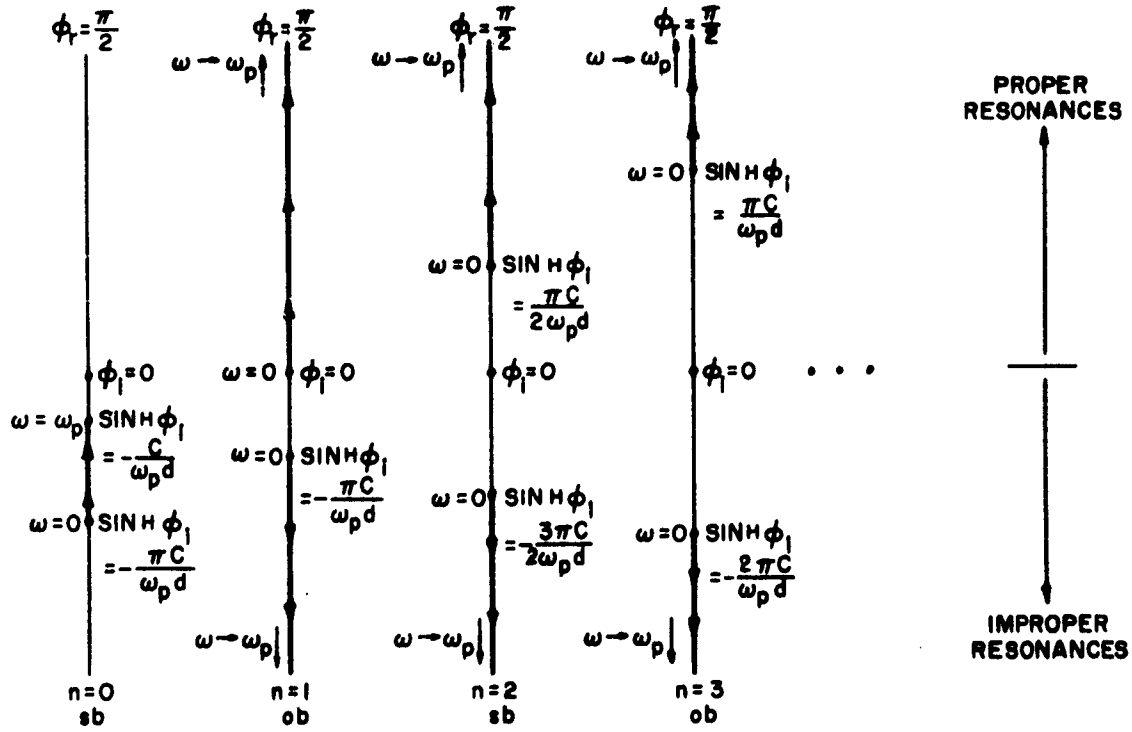

Fig. 4.10: Surface wave pole loci in the φ - plane

The location of the leaky wave loci in the φ - plane is a more complicated matter. In this case

$$p = \pm \frac{n\pi}{2} \pm j \tanh^{-1} \sqrt{\epsilon_p} \quad , \tag{4-45}$$

and

$$q = \mp \frac{n\pi}{2\sqrt{\epsilon_p}} - j \frac{1}{\sqrt{\epsilon_p}} \tanh^{-1} \sqrt{\epsilon_p} \, . \tag{4-46}$$

Equations (4-42) can then be written

$$k_o d \cos \varphi_r \cosh \varphi_i = \pm \frac{n\pi}{2\sqrt{\epsilon_p}} \quad , \tag{4-47a}$$

$$k_o d \sin \varphi_r \sinh \varphi_i = - \frac{1}{\sqrt{\epsilon_p}} \tanh^{-1} \sqrt{\epsilon_p} \quad , \tag{4-47b}$$

From equation (4-47b) it can be concluded that, since $\frac{1}{\sqrt{\epsilon_p}} \tanh^{-1} \sqrt{\epsilon_p} \geq 0$, leaky wave poles will map into the strips $0 < \varphi_r < \pi$, $\varphi_i < 0$ and $-\pi < \varphi_r < 0$, $\varphi_i > 0$. Hence, contributions to the fields will be due only to leaky wave poles located in the region $0 < \varphi_r < \pi/2$, $\varphi_i < 0$. Also, from equation (4-47b), it is seen that the poles are located symmetrically about the origin of the φ - plane. In subsequent calculations attention will be limited to the strip $0 < \varphi_r < \pi/2$, $\varphi_i < 0$.

Next, limiting values will be calculated. Equations (4-47) can be written as

$$\cos \varphi_r \cosh \varphi_i = \frac{n\pi c}{2d\sqrt{\omega^2 - \omega_p^2}} \quad , \tag{4-48a}$$

$$\sin \varphi_r \sinh \varphi_i = - \frac{c \tanh^{-1} \sqrt{1 - (\omega_p/\omega)^2}}{d\sqrt{\omega^2 - \omega_p^2}} \tag{4-48b}$$

Also from equations (4-47) one obtains

$$q_r = \frac{n\pi}{2} \coth \left[\frac{n\pi}{2} \tan \varphi_r \tanh \varphi_i \right] . \tag{4-49}$$

Now, when q_r approaches $n\pi/2$ it follows from (4-49) that

$$\tan \varphi_r \tanh \varphi_i = \infty ,$$

and hence $\varphi_r = \pi/2$. The corresponding value of φ_i, obtained from equation (4-48b) is $\varphi_i = 0$. These limiting values correspond to $\omega = \infty$. When $\omega = \omega_p$ the limiting values, obtained from equations (4-48b) and (4-49) are given by $\varphi_r = 0$, $\varphi_i = -\infty$.

Further properties of the roots can be obtained from equation (4-48a). Note that at a given finite frequency, as n is made to increase, cosh φ_i must increase (since $0 < \cos \varphi_r < 1$ in the region of interest). This means that the poles corresponding to large n at this fixed frequency must be in the region, φ_r small and φ_i very negative. Consequently, it follows (from the shape of the steepest descent curve in Fig. 4.6) that a finite number of leaky wave poles will contribute to the field for a given angle of observation $0 < \theta < \pi/2$.

The above information yields a qualitative picture of the leaky wave pole loci in the φ - plane. It is possible to obtain a more exact picture by graphical calculation. Thus equations (4-47) and (4-49) can be used to obtain an explicit equation for the pole loci, namely

$$\sinh \left(\frac{n\pi}{2} \tan \varphi_r \tanh \varphi_i \right) = - \left(\frac{n}{4}\right) \left(\frac{\lambda_p}{a}\right) \sec \varphi_r \operatorname{sech} \varphi_i , \qquad (4\text{-}50)$$

where λ_p is the plasma wavelength. Equation (4-50) can be solved graphically to yield quantitative results for the poles in the φ - plane. The qualitative information obtained above, together with a knowledge of the quantitative behavior of the pole loci obtained from equation (4-50), shows that the leaky wave loci in the φ - plane are as illustrated in Fig. 4-11 a and b. The steepest descent path for $\theta = \pi/2$ is shown dotted.

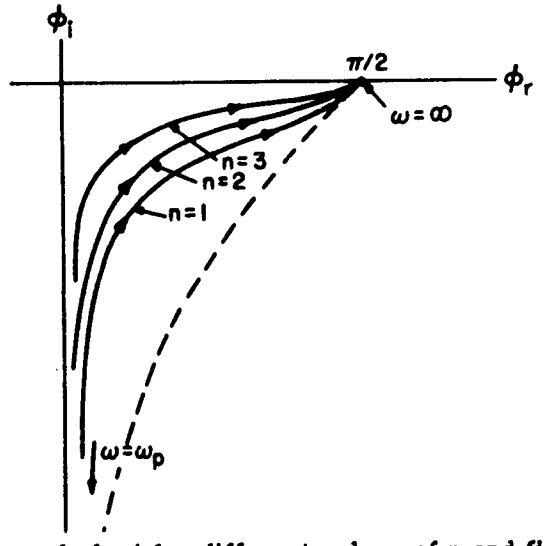

Fig. 4.11a: Leaky wave pole loci for different values of n and fixed $\frac{\lambda_p}{d}$.

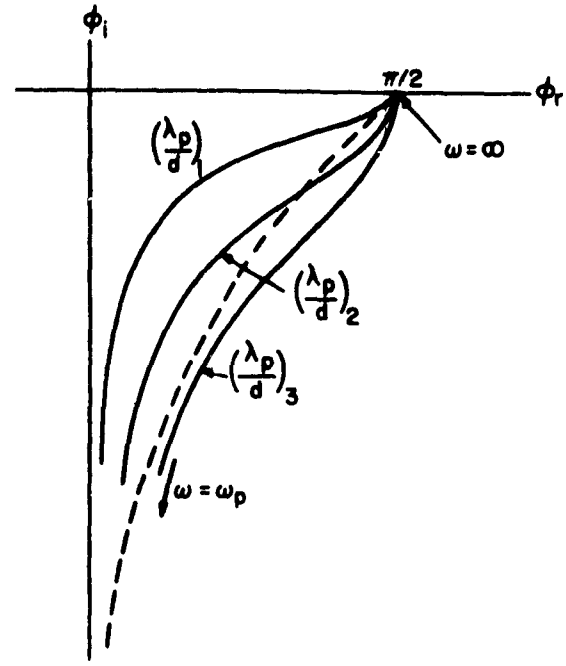

Fig. 4.11b: Leaky wave pole loci for same value of n and $(\frac{\lambda_p}{d})_1 < (\frac{\lambda_p}{d})_2 < (\frac{\lambda_p}{d})_3$.

3. Some Properties of the Surface Waves

One of the unexpected features of the surface wave resonances is the fact that an infinite number of these exist and give rise to residue terms at any frequency below the plasma frequency. Actually this result is not so strange when one considers the dispersion relations given by equations (4-3) and (4-5). These are plotted in Fig. 4.12, on the same set of axes, for $\omega < \omega_p$. It is seen from an examination of the curves in Fig., 4.12 that an infinite number of imaginary values of k_z will satisfy both curves for real values of ξ and $\varkappa_z$. Another point of interest is the fact that the vector drawn from the origin to a point on the plasma dispersion curve (i. e. the wavenumber) tends to become collinear with the line $\varkappa_z = \frac{1}{|\epsilon_p|}\xi$ for higher surface wave resonances (higher values of ξ). It is also noted that for the higher resonances the values of ξ and $\varkappa_z$ are larger and hence the electrical length of the slab $\varkappa_z d$ increases with n.

The dispersion curves for the individual surface waves can be easily obtained from the results which have already been derived. Hence, using the fact that

$$\epsilon_p = 1 - (\frac{\omega_p}{\omega})^2 = 1 - (\frac{\lambda}{\lambda_p})^2$$

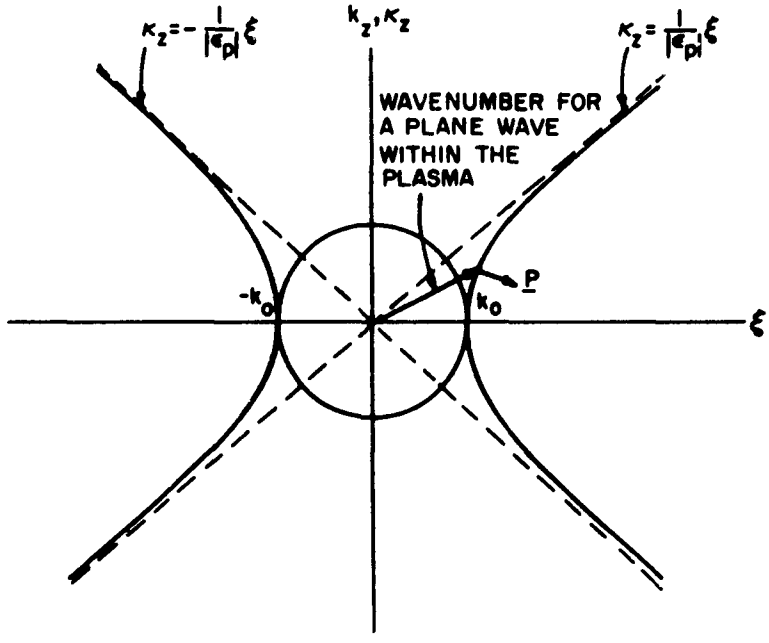

Fig. 4.12: Plot of dispersion relations for free space and for the plasma when $\omega < \omega_p$.

and introducing the results given in equations (4-34) one obtains

$$\frac{\lambda}{\lambda_p} = \begin{cases} -\sec p_r \quad , \text{(s b)} \quad , & \text{(4-51a)} \\ \csc p_r \quad , \text{(o b)} \quad . & \text{(4-51b)} \end{cases}$$

Now, introducing equations (4-38) into equation (4-5) one obtains

$$\frac{\lambda}{\lambda_x} = \begin{cases} \sqrt{1 + (\frac{\lambda p}{d})^2 (\frac{p_r}{2\pi})^2 \csc^2 p_r} \quad , \text{(s b)} \, , & \text{(4-52a)} \\ \sqrt{1 + (\frac{\lambda p}{d})^2 (\frac{p_r}{2\pi})^2 \sec^2 p_r} \quad , \text{(o b)}. & \text{(4-52b)} \end{cases}$$

Equations (4-51) and (4-52) are the parametric equations of the surface wave dispersion curves. The range of values on the parameter p_r can be obtained from Fig. 4.7, with the result that the dispersion curves can be sketched as shown in Fig. 4.13.

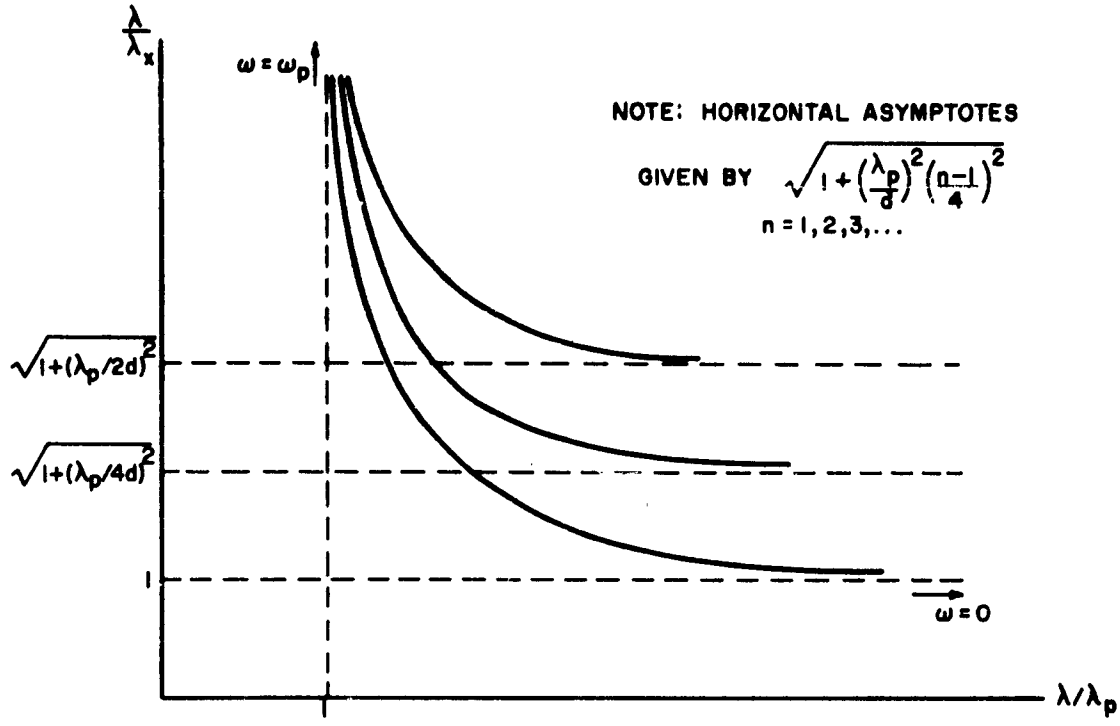

Fig. 4.13: Surface wave dispersion curves.

The slopes of the curves in Fig. 4.13 are all negative. Since the group velocity is related to the negative of the slopes of these curves, the phase and group velocities are both positive and the waves are all forward in the x direction.

The spatial variation of the surface waves is sinusoidal within the slab and exponentially decaying outside the slab. If, in the source free case, I_d is the amplitude of the current function at z = d the field distribution can be written as follows:

s b case

(a) $0 \leq z < d$

$$E_x = \frac{I_d}{\sqrt{2\pi}} \frac{\varkappa_z}{j\omega\varepsilon_o\varepsilon_p} e^{-j\xi x} \frac{\sin \varkappa_z z}{\cos \varkappa_z d},$$

$$H_y = \frac{I_d}{\sqrt{2\pi}} e^{-j\xi x} \frac{\cos \varkappa_z z}{\cos \varkappa_z d}, \qquad (4\text{-}53a)$$

$$E_z = -\frac{I_d}{\sqrt{2\pi}} \frac{\xi}{\omega\varepsilon_o} e^{-j\xi x} \frac{\cos \varkappa_z z}{\cos \varkappa_z d},$$

(b) $z > d$

$$E_x = \frac{I_d}{\sqrt{2\pi}} \frac{\kappa_z}{j\omega\epsilon_o\epsilon_p} \frac{\sin \kappa_z d}{\cos \kappa_z d} e^{-j\xi x} e^{-|k_z|(z-d)},$$

$$H_y = \frac{I_d}{\sqrt{2\pi}} e^{-j\xi x} e^{-|k_z|(z-d)}, \qquad (4\text{-}53b)$$

$$E_z = -\frac{I_d}{\sqrt{2\pi}} \frac{\xi}{\omega\epsilon_o} e^{-j\xi x} e^{-|k_z|(z-d)},$$

o b case

(a) $0 \leq z < d$

$$E_x = \frac{I_d}{\sqrt{2\pi}} \frac{\kappa_z}{j\omega\epsilon_o\epsilon_p} e^{-j\xi x} \frac{\cos \kappa_z z}{\cos \kappa_z d},$$

$$H_y = \frac{I_d}{\sqrt{2\pi}} e^{-j\xi x} \frac{\sin \kappa_z z}{\sin \kappa_z d}, \qquad (4\text{-}54a)$$

$$E_z = -\frac{I_d}{\sqrt{2\pi}} \frac{\xi}{\omega\epsilon_o} e^{-j\xi x} \frac{\sin \kappa_z z}{\sin \kappa_z d},$$

(b) $z > d$

$$E_x = \frac{I_d}{\sqrt{2\pi}} \frac{\kappa_z}{j\omega\epsilon_o\epsilon_p} \frac{\cos \kappa_z d}{\sin \kappa_z d} e^{-j\xi x} e^{-|k_z|(z-d)},$$

$$H_y = \frac{I_d}{\sqrt{2\pi}} e^{-j\xi x} e^{-|k_z|(z-d)}, \qquad (4\text{-}54b)$$

$$E_z = -\frac{I_d}{\sqrt{2\pi}} \frac{\xi}{\omega\epsilon_o} e^{-j\xi x} e^{-|k_z|(z-d)}.$$

One of the interesting consequences of the anisotropy in the present problem is that the z component of the electric field is continuous over the plasma-free space interface. As a result power travels in the same direction both inside and outside the plasma. This result follows from the fact that the only real component of the Poynting vector is $P_x = -E_z H_y^*$. It is interesting to point out that in the case of the isotropic

plasma slab, which has been thoroughly studied by Tamir[11], power travels in opposite directions in the plasma and free space regions. Again, this result occurs because of the discontinuity in E_z over the interface.

One more point of interest should be mentioned in connection with power. If the fields within the slab are interpreted as being composed of plane waves which are reflected back and forth within the slab, then the wavenumber for a particular plane wave is given by the vector which is constructed in Fig. 4.12. The average power flow vector $\underline{P} = R_e (\underline{E} \times \underline{H}^*)$ is directed normal to the dispersion curve[8,20]. It is seen from Fig. 4.12 that the angle between the wavenumber and $\underline{P}$ is less than 90°. It is pointed out that the net power transfer is in the x direction even though $\underline{P}$ has a component in the negative z direction. This follows from the fact that when the plane wave is reflected at the plasma interface the resulting Poynting vector will have a component in the positive z direction. Hence, the Poynting vectors due to the two plane waves combine to give a net component in the x-direction.

4. Some Properties of the Fields Above the Slab

Some of the properties of the fields due to the residue terms, and their relationship to the geometry of the structure will now be considered. Since the general properties of the surface and leaky wave fields are essentially independent of the source location the discussion will be limited to the case where the line source is located at z = 0. Also, since the characteristics of such waves have been discussed in great detail elsewhere,[10,11] the presentation here will be brief.

From equation (4-26) it is seen that the residue fields vary as

$$f(r, \theta) = e^{-jk_o r \cos(\varphi_p - \theta)} \tag{4-55}$$

where

$$\varphi_p = \frac{\pi}{2} + j\varphi_{ip}$$

for the surface waves, and

$$\varphi_p = \varphi_{rp} + j\varphi_{ip}$$

for the leaky waves. Now, considering the surface waves separately, it is seen that the constant phase surfaces are perpendicular to the x-axis and given by

$$r \cos\left(\frac{\pi}{2} - \theta\right) = \text{constant},$$

while the constant amplitude surfaces are parallel to the x-axis and given by

$$r \sin\left(\frac{\pi}{2} - \theta\right) = \text{constant}.$$

It follows that if a surface wave is observed along a plane of constant phase the amplitude decreases exponentially with the distance from the interface. These remarks are illustrated in Fig. 4.14. The angle θ_o is the angle of observation at which the

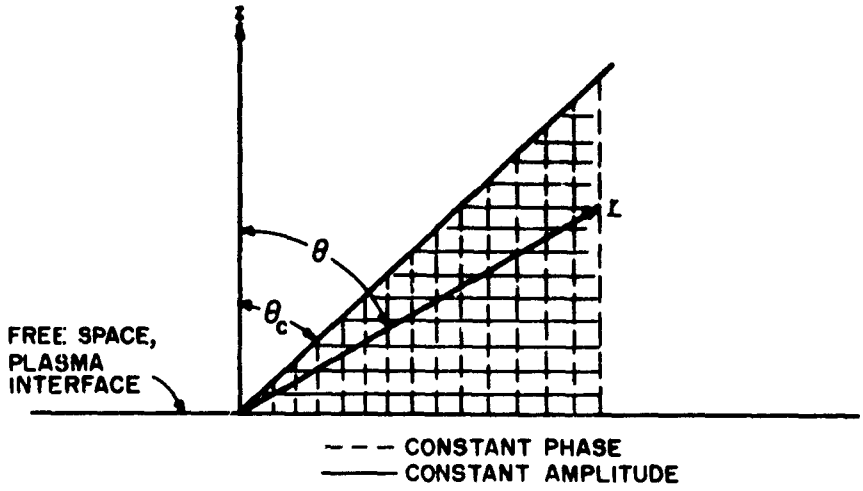

Fig. 4.14: Constant phase and amplitude surfaces for the surface wave field above the slab.

residue field for a particular surface wave pole is first observed, i.e., the angle for which the steepest descent curve intercepts the pole.

Remarks which are similar to the above can also be made for the leaky waves. In this case $\varphi_{rp} < \theta$ and the constant phase surfaces are given by

$$r \cos (\theta - \varphi_{rp}) = \text{constant},$$

while the constant amplitude surfaces are given by

$$r \sin (\theta - \varphi_{rp}) = \text{constant}.$$

It follows from these results and equation (4-55) that the leaky wave decreases exponentially with distance from the wave vector $\underline{k}_p$ which is indicated in Fig. 4.15. This last result implies growth in the direction perpendicular to the slab and decay in the direction parallel to the slab. These remarks are illustrated in Fig. 4.15. One more fact is of interest and this follows from the expression for the phase velocity for a surface or leaky wave

$$v_p = \frac{c}{\cos (\theta - \varphi_{rp}) \cosh \varphi_{ip}}.$$

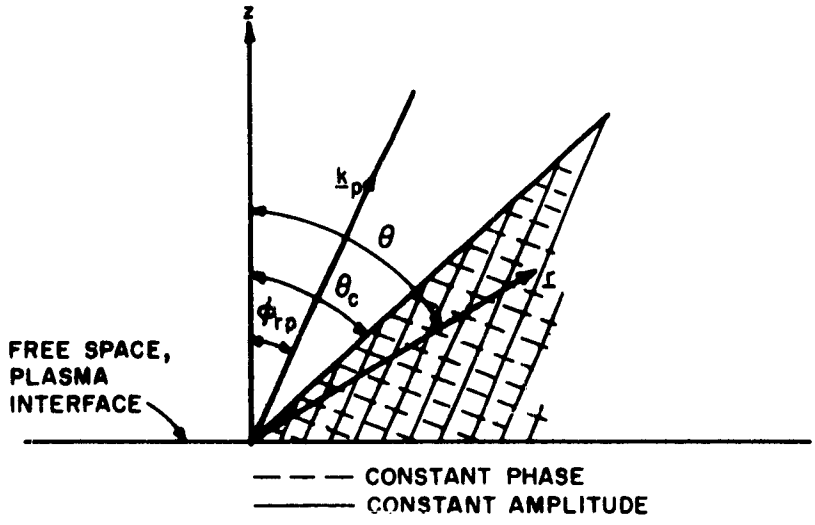

Fig. 4.15: Constant phase and amplitude surfaces for the leaky wave field above the slab.

It is seen that the surface waves are slow waves, while the leaky waves are fast waves.

REFERENCES

1. R. E. Collin, Field Theory of Guided Waves, McGraw Hill Book Company, Inc., pp. 97-116, New York, 1960.

2. R. E. Collin, "A Simple Artificial Anisotropic Dielectric Medium", I. R. E. Trans., vol. MTT-6, pp. 206-209; April, 1958.

3. G. Joos, Theoretical Physics, 2d ed., Blackie and Sons, Ltd., Glasgow, 1951.

4. G. Estrin, "The Effect of Anisotropy in a Three-Dimensional Array of Conducting Disks", Proc. I. R. E., vol. 39, pp. 821-826; July, 1951.

5. G. Estrin, "The Effective Permeability of an Array of Thin Conducting Disks", Journal of Appl. Phys., vol. 21, pp 667-670; July, 1950.

6. E. Arbel and L. B. Felson, "On Electromagnetic Green's Functions for Uniaxially Anisotropic Regions", Electrophysics Dept., Polytechnic Institute of Brooklyn, Report PIBMRI-985-61; Feb., 1962.

7. E. Arbel, "Radiation from a Point Source in an Anisotropic Medium", Microwave Res. Inst., Polytechnic Institute of Brooklyn, Report PIBMRI-861-60; Nov., 1960.

8. L. B. Felson, "Radiation from a Uniaxially Anisotropic Plasma Half Space", Electrophysics Dept., Polytechnic Institute of Brooklyn, Report PIBMRI-1058-62; August, 1962.

9. L. B. Felson and N. Marcuvitz, "Modal Analysis and Synthesis of Electromagnetic Fields", Polytechnic Institute of Brooklyn, Microwave Res. Inst., Reports R-446-55 (a, b), R-726-59, R-776-59.

10. S. Barone, "Leaky Wave Contributions to the Field of a Line Source Above a Dielectric Slab", Polytechnic Institute of Brooklyn, Microwave Res. Inst., Report PIBMRI 532-56; Nov. 1956.

11. T. Tamir, "The Electromagnetic Field of a Source Excited Plasma Slab", Polytechnic Institute of Brooklyn, Microwave Res. Inst., Report PIBMRI-932-61; Sept. 1961.

12. T. Tamir, "Leaky Wave Contributions to the Field of an Electric Line Source Above a Plasma Slab", Polytechnic Institute of Brooklyn, Microwave Res. Inst., Report PIBMRI-845-60; Nov. 1960.

13. T. Tamir, "The Influence of Complex Waves on the Radiation Field of a Slot-Excited Plasma Layer", Polytechnic Institute of Brooklyn, Microwave Res. Inst., Report PIBMRI-959-61; Nov. 1961.

14. B. Friedman, Principles and Techniques of Applied Mathematics, J. Wiley and Sons, Inc., New York, 1957.

15. L. D. Landau and E. M. Lifschitz, Electrodynamics of Continuous Media, Pergamon Press, New York, 1960.

16. J. G. Linhart, Plasma Physics, Interscience Publishers, Inc., New York, 1960.

17. K.G. Budden, The Wave-Guide Mode Theory of Wave Propagation, Prentice-Hall, Inc., New Jersey, 1961.

18. A. Erdelyi, Asymptotic Expansions, Dover Publications, Inc., New York, 1956.

19. N. Marcuvitz and J. Schinger, "On the Representation of the Electric and Magnetic Fields Produced by Currents and Discontinuities in Waveguides", J. Appl. Phy., 22, pp 806-819, 1951.

20. K.G. Budden, Radio Waves in the Ionosphere, Cambridge University Press, 1961.